Marine Geology 416 (2019) 105998

Contents lists available at ScienceDirect

Marine Geology

journal homepage: www.elsevier.com/locate/margo

Sandbanks, sandwaves and megaripples on Spitsbergenbanken, Barents Sea

Valérie K. Bellec[a,*], Reidulv Bøe[a], Lilja R. Bjarnadóttir[a], Jon Albretsen[b], Margaret Dolan[a], Shyam Chand[a], Terje Thorsnes[a], Frank W. Jakobsen[a], Chantel Nixon[c], Liv Plassen[a], Henning Jensen[a], Nicole Baeten[a], Heidi Olsen[a], Sigrid Elvenes[a]

[a] Geological Survey of Norway (NGU), Postbox 6315, Torgarden, 7491 Trondheim, Norway
[b] Institute of Marine Research (IMR), Postbox 1870, Nordnes, N-5870 Bergen, Norway
[c] NTNU, NO-7491 Trondheim, Norway

ARTICLE INFO

Editor: Michele Rebesco

Keywords:
Megaripple
Sandwave
Sandbank
Barents Sea
Spitsbergenbanken
High-latitude continental shelf

ABSTRACT

Recently acquired multibeam echosounder data from the shallowest part (26–53 m depth) of Spitsbergenbanken in the western Barents Sea reveal a variety of bedforms, including megaripples, sandwaves and sandbanks. The bedforms exhibit varying degrees of superimposition and differ in their age of formation and present depositional regime, being either active or moribund. These are the first observations of co-occurring current induced bedforms in the western Barents Sea and provide evidence of a high energy environment in the study area. The bedforms indicate both sediment erosion and transport and confirm that there is enough sand available in this area to maintain them. Such conditions are not known to be common in the western Barents Sea and reflect the unique oceanographic and benthic environment of Spitsbergenbanken.

1. Introduction

Spitsbergenbanken is a large bank in the Barents Sea, between the island of Bjørnøya and Svalbard. About 40% of the bank is < 100 m deep. Available data indicate that the seabed of the bank is dominated by sandy and gravelly sediments (Lepland et al., 2014). MAREANO (www.mareano.no) is a Norwegian seabed mapping programme started in 2006 to ameliorate the knowledge of the Norwegian sea bottom. In the framework of this programme, high resolution multibeam echosounder data were acquired from the shallowest part of the bank (Fig. 1). These new data allowed identifying a large variety of bedforms varying from sand ripples to megaripples and sandwaves to sandbanks (Figs. 1 and 2). An oceanographic model supplied information on the physical environment between 74° and 84° N, including Spitsbergenbanken.

Sandwaves and sandbanks have been extensively studied, especially in the North Sea (e.g. Bellec et al., 2010; Collins et al., 1995; Trentesaux et al., 1999), because they may represent a hazard to navigation and offshore constructions. They feature sand transported and deposited by bottom currents, but their orientation relative to the bottom current flow direction varies. Sandwaves with ripples and megaripples are transverse bedforms, with their crest generally oriented perpendicular to the flow, while sandbanks are longitudinal bedforms with their long axis generally parallel or oblique (up to 20°) to the regional peak flow direction (Belderson et al., 1982).

On the Norwegian margin, sandwaves have been described from glacial troughs (Bøe et al., 2009; Elvenes et al., 2016) and along the continental slope (Bøe et al., 2015; King et al., 2014). Sandwaves have also been observed in shallow areas of the Svalbard continental shelf (Ottesen and Dowdeswell, 2009) but so far, sandwaves and sandbanks have not been described on the shallow banks in the western Barents Sea. Megaripples on continental shelves, with the exception of the coastal zone, have been very little studied and no previous papers show a similar variety of megaripples as described in our study area.

2. Geological, bathymetric and oceanographic setting

The Barents Sea was entirely covered by ice during the maximum of the last glaciation at about 24 cal. ka BP. Deglaciation commenced around 18 cal. ka BP leaving Spitsbergenbanken free of grounded ice about 14 cal. ka BP (Hughes et al., 2016). This was followed by a period of deposition of current transported sediments from more distal sources, recorded in e.g. large drifts in Kveithola, a trough located north of Bjørnøya Island (13.1–10.3 cal. ka BP) (Bjarnadóttir et al., 2013; Rüther et al., 2012). Younger sand accumulations reported from several locations in the region have been linked to an increase in bottom current strength and erosion between 11.2 and 8.8 cal. ka BP (Bjarnadóttir et al., 2013; Jensen et al., 2002; Lantzsch et al., 2017; Rüther et al., 2012).

* Corresponding author.
E-mail address: valerie.bellec@ngu.no (V.K. Bellec).

https://doi.org/10.1016/j.margeo.2019.105998
Received 12 April 2019; Received in revised form 17 July 2019; Accepted 19 July 2019
Available online 20 July 2019

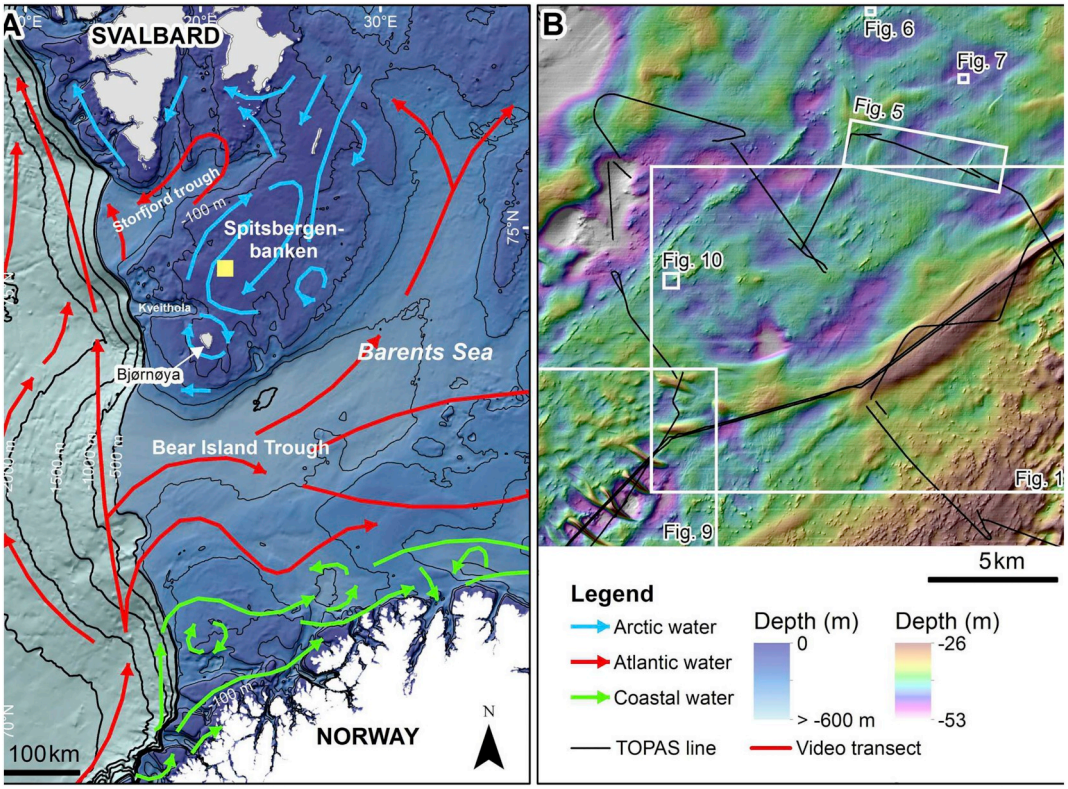

Fig. 1. A) Overview map with location of study area (yellow square) and main oceanographic currents (from Loeng, 1989) (IBCAO bathymetry data, Jakobsson et al., 2012). B) Multibeam bathymetry (5 m grid) of the study area with sandwaves in the southwest and sandbanks in the central part. (For interpretation of the references to colour in this figure legend, the reader is referred to the web version of this article.)
Multibeam bathymetry from MAREANO (www.mareano.no).

Strong inflow of warm and saline Atlantic Water into the Barents Sea took place about 9 to 6 cal. ka BP during the Holocene thermal maximum (e.g. Rasmussen et al., 2014; Risebrobakken et al., 2011). The flux of Atlantic Water started to decrease during the late Holocene (4–2 cal. ka BP) together with an atmospheric cooling (Neoglacial cooling; Ślubowska-Woldengen et al., 2008) also documented around Kveithola (Zecchin et al., 2016).

Spitsbergenbanken is presently under the influence of the East Spitsbergen Current that transports a mixture of Arctic Water and Polar Front Water (Skogseth et al., 2005; Ślubowska-Woldengen et al., 2008). Oceanographic studies and modelling show that the study area is located close to the center of a clockwise current gyre formed by cold Polar Water (Fig. 1) (Loeng, 1989; Slagstad and McClimans, 2005). Tidal currents are particularly strong over the shallow bank, with maximum speed of up to 1 m/s, tidal range of 20–40 cm and a phase angle of about 330° on the top of the bank (Gjevik et al., 1994; Gjevik, 2008). Around Spitsbergenbanken, mean wind stress comes from the east (Weigel, 2005).

The study area is located in the shallowest part of Spitsbergenbanken, at depths ranging from −26 to −53 m. Ocean depths in the area have varied since the deglaciation, due to crustal uplift and eustatic sea level rise. However, the details of these changes are at present not known. From Bjørnøya island (about 70–80 km from the study area), observations indicate that eustatic sea level rise since deglaciation has exceeded crustal uplift in this area (Salvigsen and Slettemark, 1995).

3. Methods

Ages cited in this paper are reported as given in references, meaning that calibration methods may differ in some cases. However, this does not significantly affect the main conclusions presented here.

The study area was mapped in 2016 by MAREANO (www.mareano.no) using Kongsberg EM2040 Dual Head multibeam echosounder (200–400 kHz). Bathymetry data were processed by using QPS Qimera and quality controlled by Kartverket. Kartverket also produced the terrain models. Backscatter data were processed by NGU using QPS FMGT software. The data density was sufficient for gridding the bathymetry at 20 cm, allowing detailed analysis of seabed features. The exceptional quality and high resolution of the datasets allowed us to resolve bedforms as small as 4 cm high and 1 m long.

On a MAREANO sampling cruise with R/V G.O. Sars in 2017, eleven video transects of 700 m length were acquired in an area of about 450 km^2. These video surveys were performed using a towed video platform (Buhl-Mortensen et al., 2009). A preliminary interpretation of the seafloor sediments was done during the acquisition of the video transects.

During the same cruise, about 75 km of high-resolution seismic lines (Kongsberg TOPAS PS 018 parametric sub-bottom profiler, chirp modus, secondary beam frequency 0.5–6 kHz) with vertical resolution better than 1 m were acquired on transit between the video transects. In 2018, about 38 km of new seismic lines were acquired by R/V H.U. Sverdrup II (Kongsberg TOPAS PS 018). TOPAS lines were processed with the TOPAS software.

Model results from an oceanographic realization of the

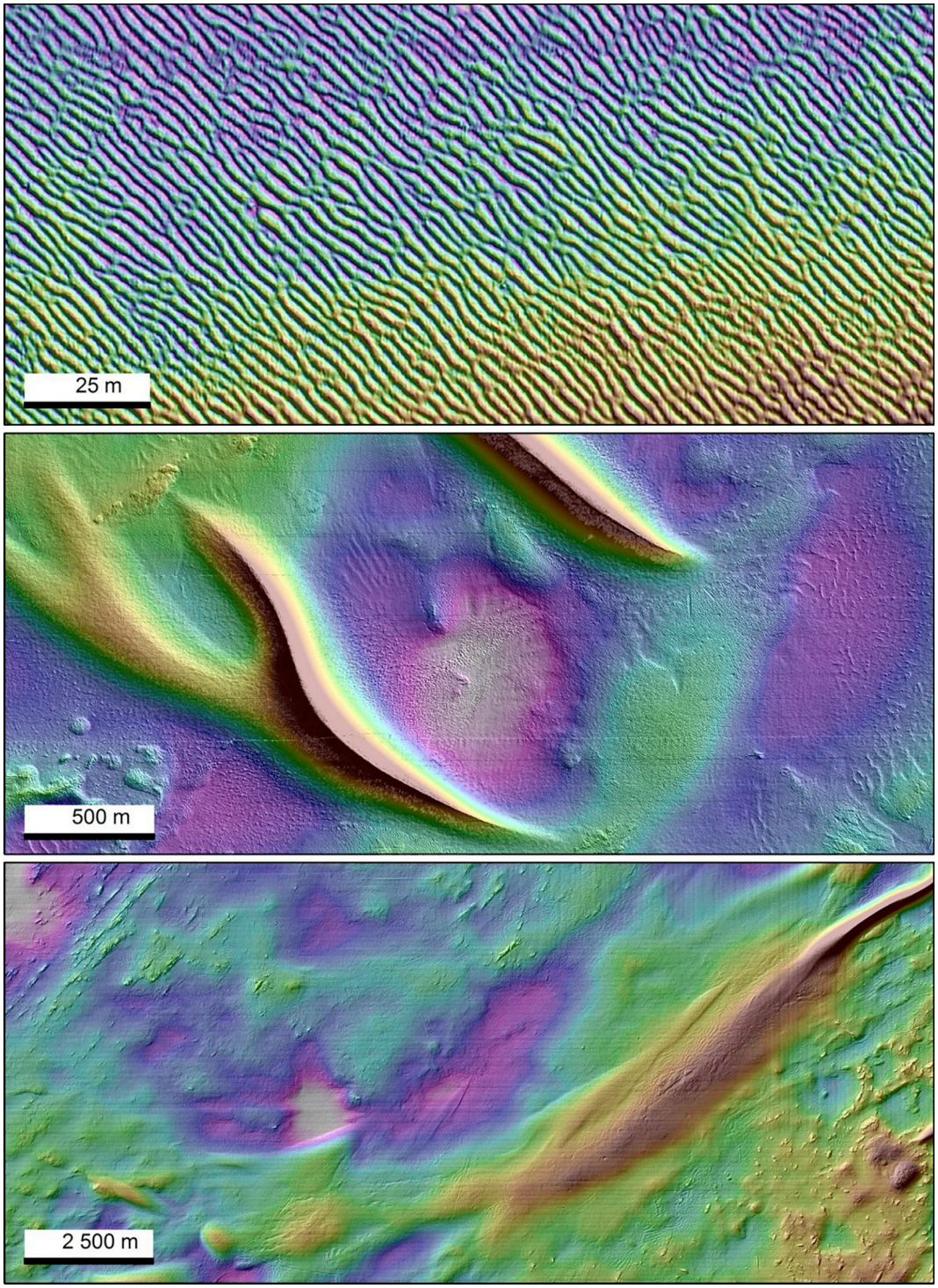

Fig. 2. Megaripples (top panel, 20 cm grid), sandwaves (middle panel, 5 m grid) and sandbanks (bottom panel, 5 m grid) in the study area. Horizontal scales and colour scales (brown (shallow) to white (deep)) are different for each panel. (For interpretation of the references to colour in this figure legend, the reader is referred to the web version of this article.)
Multibeam bathymetry from MAREANO (www.mareano.no).

Table 1
Megaripple characteristics.

Megaripple types	Crest orientation (°)	Symmetric	Height	Wavelength	Area covered (km^2)	Sediment type
Elongated – Type 1	N-S: 3–13	Yes	10–30 cm	2–3 m	85	Mostly gravel, some sand and shells
Elongated – Type 2	NW-SE: 30 (north area), 45 (south area)	No, either to the SW or to the NE	10–30 cm	2–3 m	120	Sand, gravelly sand
Elongated – Type 3	NW-SE: 340–345 generally, 310 in the east area	No, to the NE	3–4 cm in the N to 15–20 cm in the south	2–3 m in the S	Minimum 13	Sand, gravelly sand
Complex – Type 4	–		20–50 cm	3–15 m	Minimum 3 km^2	Likely sandy
Lingoid/lunate – Type 5	55	No, to the SW	25–35 cm	3–10 m	1.5	Sand (gravelly sand)

hydrodynamic conditions of the Svalbard area were retrieved from the archive documented in Hattermann et al. (2016). This Svalbard model applied 800 m × 800 m horizontal resolution and was able to provide information on the physical environment with relatively high resolution. The model was set up using the bathymetry from IBCAO.v3 (International Bathymetric Chart of the Arctic Ocean, Jakobsson et al., 2012) and was run using the numerical ocean model ROMS (Regional Ocean Modelling System; http://myroms.org) which applies a vertical topography-following coordinate. The model was forced with tidal analysis from TPXO7.2 (Egbert and Erofeeva, 2002). The model results in this study were extracted from the lowermost level, and we applied maximum current speed along with mean currents.

4. Results

Three main types of bedforms are described in this paper (megaripples, sandwaves and sandbanks; Fig. 2). These bedforms will be characterized in terms of size, morphology and location.

4.1. Megaripples

Megaripples have wavelengths from about 60 cm to > 30 m (Ashley, 1990; Reineck and Singh, 1980). Smaller current ripples are not described in this paper due to resolution limitations in the multibeam data. Three main types of megaripples occur in our study area: elongated megaripples, complex megaripples and lingoid/lunate megaripples (Table 1, Figs. 2 and 3).

The elongated megaripples include three different types showing various orientations and morphologies (Table 1, Fig. 3). Type 1 megaripples are dominant in the northwestern part of the study area (Fig. 4) but occur in most of the low-lying areas (e.g. between the smaller sandwaves). They have long, parallel, regular crests with bifurcations (Fig. 3A, B and C) typical of wave megaripples (e.g., Reineck and Singh, 1980) and N-S crest orientation.

Type 2 elongated megaripples have shorter, sinuous crests without bifurcations characteristic of current megaripples (e.g., Reineck and Singh, 1980). These megaripples are the most common and occur in a large SW-NE corridor across the middle of the study area (Fig. 4) but also on small highs, including sandwaves. They have NW-SE crest orientations with their steep slopes often facing northeast (Fig. 3D, E and F). Their orientation and shape can vary, especially around obstacles on the seafloor (Fig. 3F). They occur in both low and high areas but are larger in the south, where they also form isolated megaripples.

Type 3 elongated megaripples are smaller, without bifurcations and with NE-SW crest orientations and are interpreted as current megaripples (e.g., Reineck and Singh, 1980). They appear mostly in the east and on the sandbanks (described below), and in a few areas in the northwest (Fig. 4). In the west and the northwest, their crest orientation changes to more N-S. In the northeastern part of the area they are on the limit to be resolved in the 20 cm grid, with heights around 4 cm and wavelength around 1 m. They become higher and wider towards the south (Fig. 3G–H).

Type 4 megaripples are defined as complex megaripples with polygonal crest patterns (Fig. 3I) or ladder crest patterns (Fig. 3J) typical of interference megaripples. They mostly occur in high areas but also on small ridges of 1–2 m high (Table 1, Figs. 3I and J, and 5). They are very common in the NW-SE current megaripple corridor where they form on top of small elongated ridges. The interference megaripples are up to 50 cm high, with wavelengths up to 15 m, and are commonly surrounded by NW-SE current megaripples. Wave megaripples frequently occur north of the interference megaripples location (Fig. 6). The interference megaripples are occasionally overprinted by NW-SE current megaripples (Fig. 7).

Type 5 is lingoid to lunate megaripples. They occur around large sandwaves in the southwestern part of the study area (see below; Fig. 4). They form megaripple fields or may occur as isolated

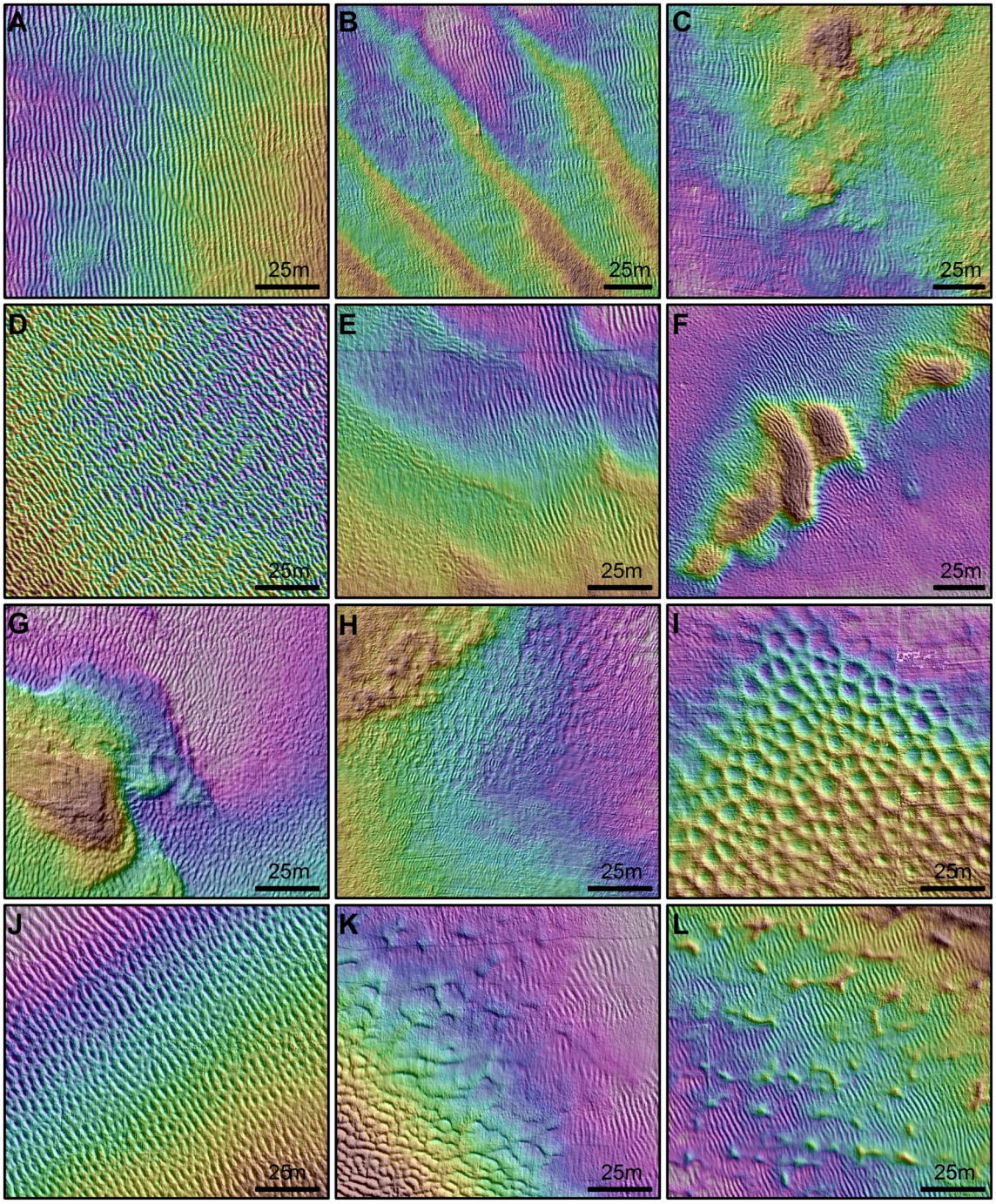

Fig. 3. Five different types of megaripples are observed in the 20 cm grid (colour scale in all panels: white is deeper, brown is shallower). North towards the top of all panels. A–C show N-S trending megaripples (type 1) interpreted as wave ripples. D–H show megaripples (types 2 and 3) likely formed by bottom currents. Megaripples (type 2) in D–F show NW-SE orientation, with panel E showing wave megaripples in low areas and NW-SE current megaripples in high areas, whereas megaripples (type 3) in G–H have NNE-SSW orientation. I-J show interference megaripples (type 4 – complex megaripples) formed by wave and bottom currents with panel I showing polygonal megaripples and panel J showing ladder megaripples. K–L display lunate/lingoid megaripples (type 5) transitional between the other types. (For interpretation of the references to colour in this figure legend, the reader is referred to the web version of this article.)
Multibeam bathymetry from MAREANO (www.mareano.no).

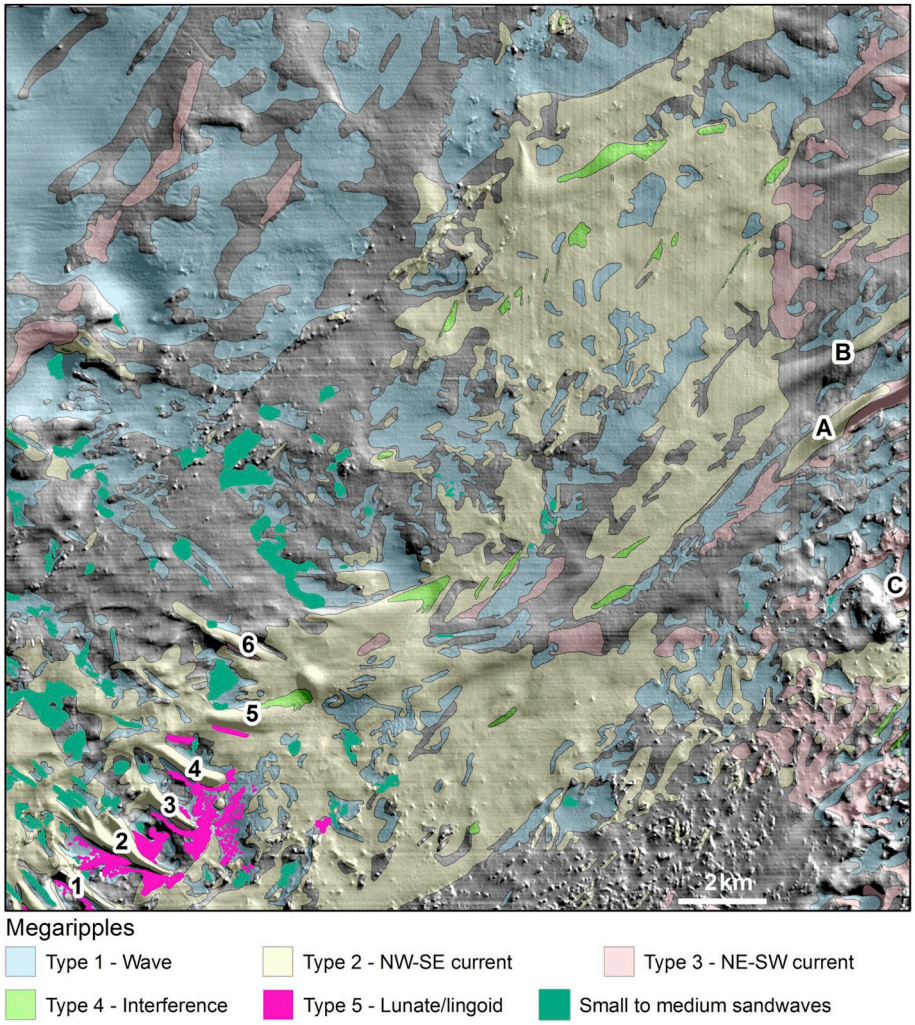

Fig. 4. Location of main types of megaripples and small to medium sandwaves in the study area. 1–4: large sandwaves; 5–6: other bedforms described in the text; A–C: sandbanks.

megaripples (Fig. 3K and L). Lingoid to lunate megaripples are often higher than the elongated megaripples and have longer wavelengths. They mostly show southward migration, but north facing megaripples occur.

4.2. Sandwaves

Four large sandwaves (1–4) with NW-SE orientation occur in the southwestern part of the study area (Fig. 8, Table 2). The three southernmost sandwaves (1–3) are the highest and display long sharp crests whereas sandwave 4 only displays a sharp crest along 250 m. It is noticeable that the crests of sandwaves 3 and 4 show a present migration direction towards the southwest (Fig. 8D and E) like the lingoid/lunate megaripples at the feet of the sandwaves (Fig. 8F) although the main body show a slight asymmetry towards the northeast. Sandwave 2 appears to be almost trochoidal in shape (Fig. 8C). On seismic profiles (Fig. 9), sandwaves 3 and 4 exhibit cross stratification showing a clear migration direction towards the northeast. The greatest water depth in the south occurs between the sandwaves and in a depression to the northeast of the sandwave area (Fig. 8A).

Smaller sandwaves surround the large sandwaves. They are even more common in the north and northwest of the sandwave area (Figs. 4 and 10). Their crests are often smooth, and they may be covered by NW-SE current megaripples, with wave megaripples in their troughs. The smaller sandwaves have generally a NW-SE crest orientation and mostly occur in the southwestern part of the study area. They are 15–220 cm high, with an average of 20–25 cm and wavelengths of a few tens of metres for the smaller sandwaves (Fig. 10). The highest of these sandwaves occur southwest and west of the large sandwaves. Smaller sandwaves mostly face northeast, but reverse direction can also occur over very short distances.

4.3. Transitional bedforms

Bedforms 5–6 (Fig. 8) occur northeast of the sandwaves. They are 4–5 m high and with E-W orientation. They are shorter, lower and have more rounded crests than the sandwaves 1–4 and their tops are largely covered by megaripples (Fig. 4). Bedform 5 exhibits cross stratification showing a clear migration direction towards the northeast, while the remnant of bedform 6 shows more aggradation than a clear progradation (Fig. 9). Both bedforms have lower internal reflector angles than the sandwaves.

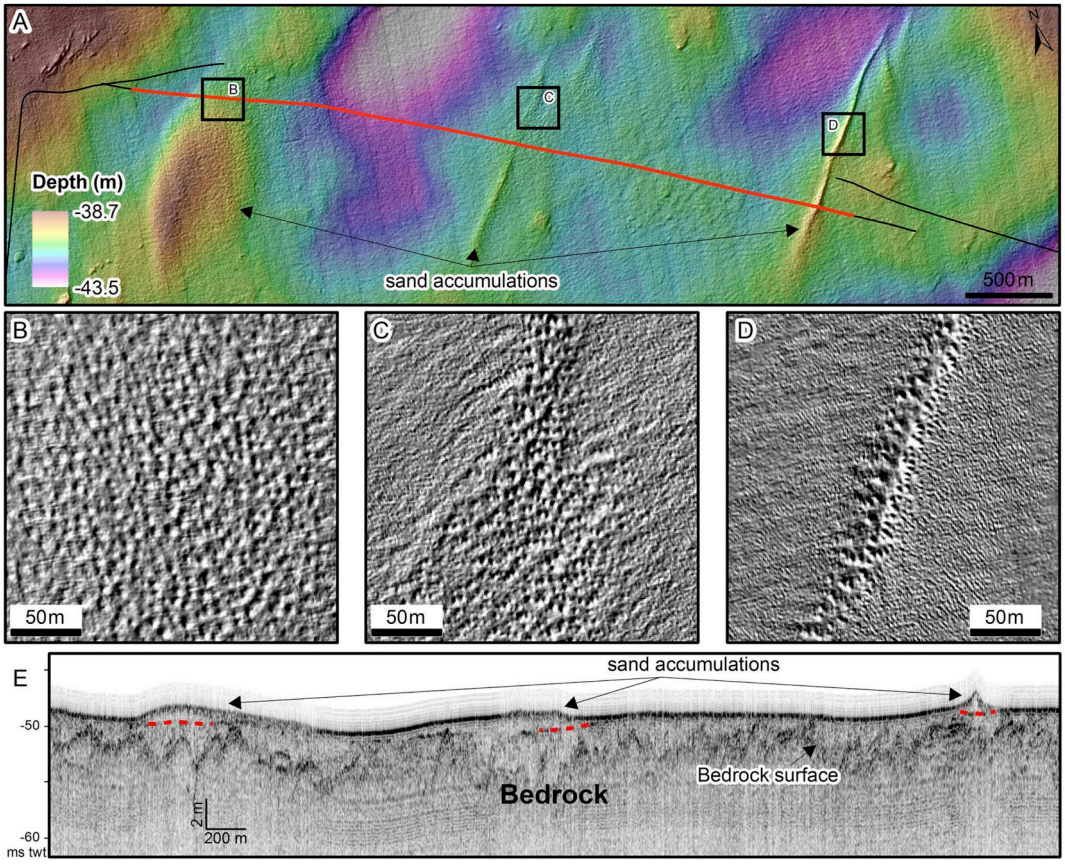

Fig. 5. A) Interference megaripples (type 4) on top of sand accumulation forming sometimes ridges. Multibeam bathymetry (5 m grid) from MAREANO (www.mareano.no). B–D: Details (1 m grid) of interference ripples in A. E) Seismic profile crossing the sand ridges. Red dotted lines are interpreted at the base of sand accumulations. See Fig. 1 for location. (For interpretation of the references to colour in this figure legend, the reader is referred to the web version of this article.)

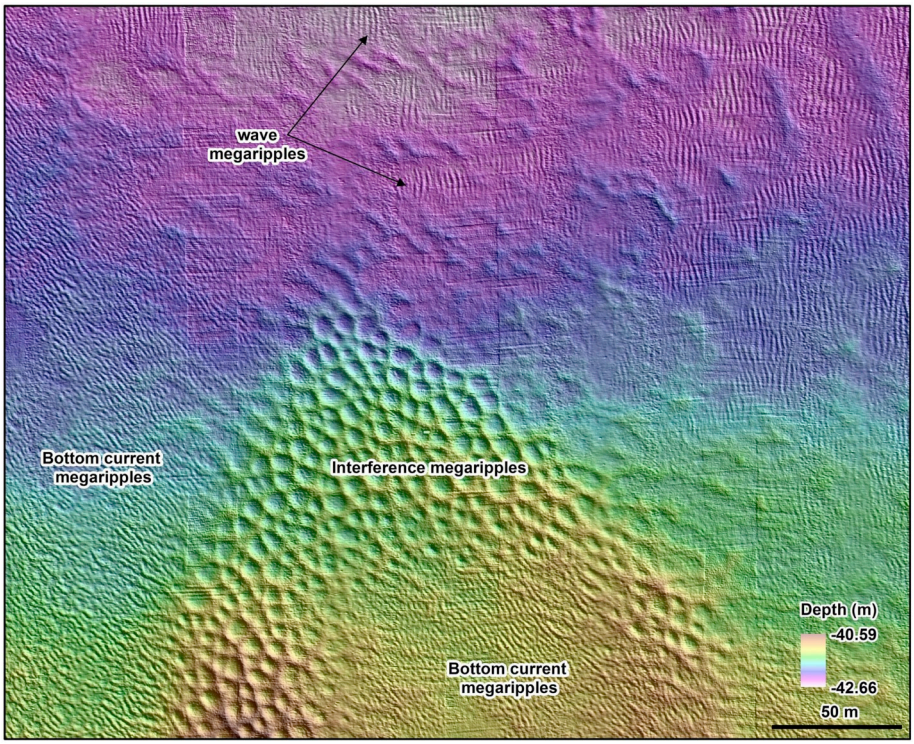

Fig. 6. Interference megaripples (type 4) surrounded by bottom current megaripples (type 2) in the south and the west and by wave megaripples (type 1) in the north and the northeast. Grid size: 20 cm. See Fig. 1 for location.
Multibeam bathymetry from MAREANO (www.mareano.no).

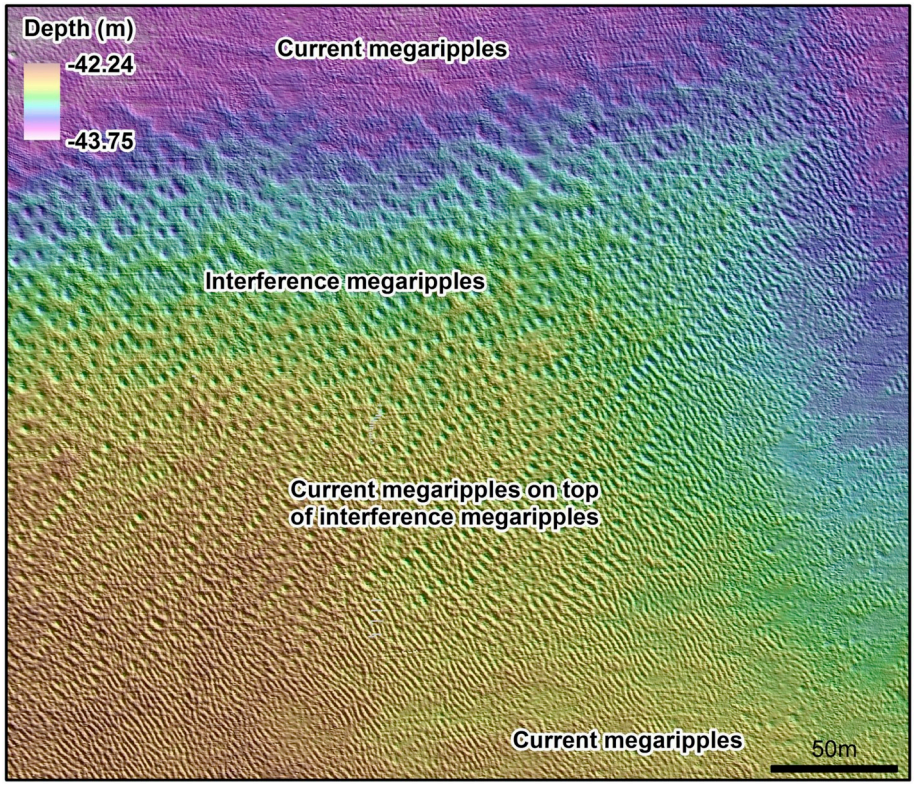

Fig. 7. Interference (type 4) megaripples partly covered by current (type 2) megaripples. Grid size: 20 cm. See Fig. 1 for location. Multibeam bathymetry from MAREANO (www.mareano.no).

4.4. Sandbanks

A SW-NE trending sandbank (A in Fig. 11) in the eastern part of the study area is up to 13 m high, > 15 km long and 300–500 m wide. It becomes narrower towards the northeast, where it has a sharp crest, while in the west it is flat-topped. Its southwestern tail is split in two (Aa and Ab in Fig. 11) where Aa links up with bedforms 5 and 6. Sandbank A comprises two units deposited on older facies interpreted as post-glacial deposits (Figs. 12–14): an older unit forming the base and tail of the bank, and a younger unit forming the narrow body in the east with a sharp crest. These two units are separated by a high amplitude reflector. Small sandwaves occur on top of the bank where the crest is sharp (Fig. 12). Buried sandwaves, covered by the younger unit, may occur on the top of the older unit, which can be traced as far as bedform 5 (Fig. 14). A sand accumulation, Ac, is located in an elongated depression along the north side of the sandbank and above its tail (Fig. 12), with an orientation of about 10–20° relative to the sandbank. The sandbank likely does not extend eastwards as it is not observed on the easternmost seismic line (Fig. 14D).

Parallel to sandbank A, sandbank B (Fig. 11) has a rounded crest, is 4–5 m high, 300–500 m wide and > 5300 m long. Sandbanks A and B are separated by a depression partly covered by unit Ac. Sandbank A appears to migrate towards the northwest (Fig. 12). A third sandbank (C) occurs south of sandbank A. Its western end is observed in the multibeam data (Fig. 14C), and the sand accumulation likely extends eastwards as a deposit observed on a seismic line (Fig. 14E). It shows a smooth crest both on multibeam (Fig. 14C) and on the seismic line (Fig. 14E).

4.5. Seabed sediments

Backscatter data (Fig. 15) have been used to map the seabed sediments (Bellec et al., 2018; Fig. 16). Sediments occur in SW-NE-trending accumulations which can be described as sand patches according to the classification of Belderson et al., 1982. These accumulations may be regular and parallel (Fig. 15B) or longer and less regular (e.g. SP1–SP3 in Fig. 15A). SP1 is at least 10 km long, up to 3.5 km wide, and has a general thickness of 1–1.5 m, but can reach 2.5 m. SP2 is about 2 km long, 2.5 km wide, and is a few centimetres to a few decimetres thick. SP3 is > 16 km long, about 3 km wide, but only a few centimetres to a few decimetres thick. SP2 and SP3 are difficult to observe in the bathymetry data.

Backscatter values are high on the southern flanks of the large sandwaves and low on their northern flanks (Fig. 15B). Small sandwaves display lower backscatter than the seabed they migrate across. In the example in Fig. 15C, wave megaripples with high backscatter occur between small sandwaves with lower backscatter.

Video observations are of variable quality due to poor visibility in the water column. Strong currents and sand ripples on the bottom were observed in most of the video lines. The seabed is mostly covered by gravelly sand and sandy gravel (Fig. 16). Patches of sand/shell sand occur in some areas, especially on sandbank B and in the Ac area (Figs. 16, 17A). Sandbank A and the sandwaves are mostly covered by gravelly sand (2–30% gravel).

The videos show that N-S trending wave megaripples often comprise sandy gravel (Fig. 17F) while NW-SE and NE-SW current megaripples comprise gravelly sand or sand (Fig. 17C–E). Interference and lunate/lingoid megaripples comprise mostly sand, while the latter may also

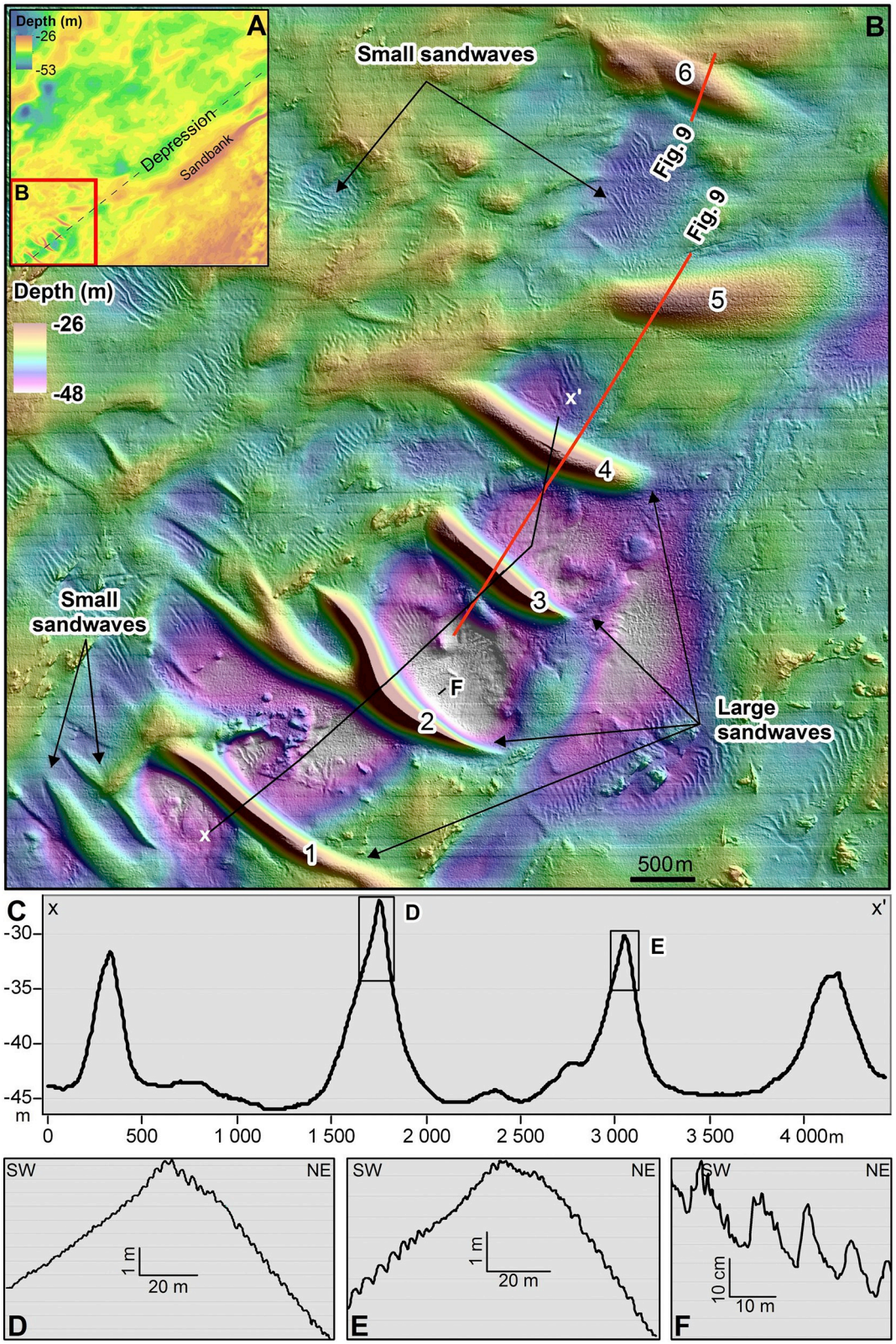

Fig. 8. Details of large (1–4) and smaller sandwaves in the study area. A) Location of B. Bedforms 5 and 6 show characteristics and orientations different from sandwaves 1–4. C) Depth profiles of sandwaves 1–4. D–E) Depth profiles of the crests of sandwaves 2 and 3 show small sandwave crests facing south. Location in panel C. F) Lingoid megaripples facing south in the trough between sandwaves 2 and 3. Location in panel B. Grid size: 5 m. See Fig. 1 for location. Multibeam bathymetry from MAREANO (www.mareano.no).

Table 2
Characteristics of sandwaves and large bedforms.

Bedform	Maximum water depth (m)	Height (m)	Crest length (m)	Crest shape and orientation	Sandwave width (m)	Width/height ratio	Comment
1	44	12.5	> 2200	Sharp along 1500 m – NW-SE	300	24	
2	45.5	19	2100	Sharp along 1700 m – NW-SE	500	26	Divided in 3 sandwaves
3	44	14	1400	Sharp along 1000 m – NW-SE	400	29	
4	43	9.5	1800	Sharp along 250 m – NW-SE	400	42	
5	40	4	1800	Rounded – E-W	370–700	92	Larger in the east
6	41	5	1500	Rounded – NW-SE	380–480	76	

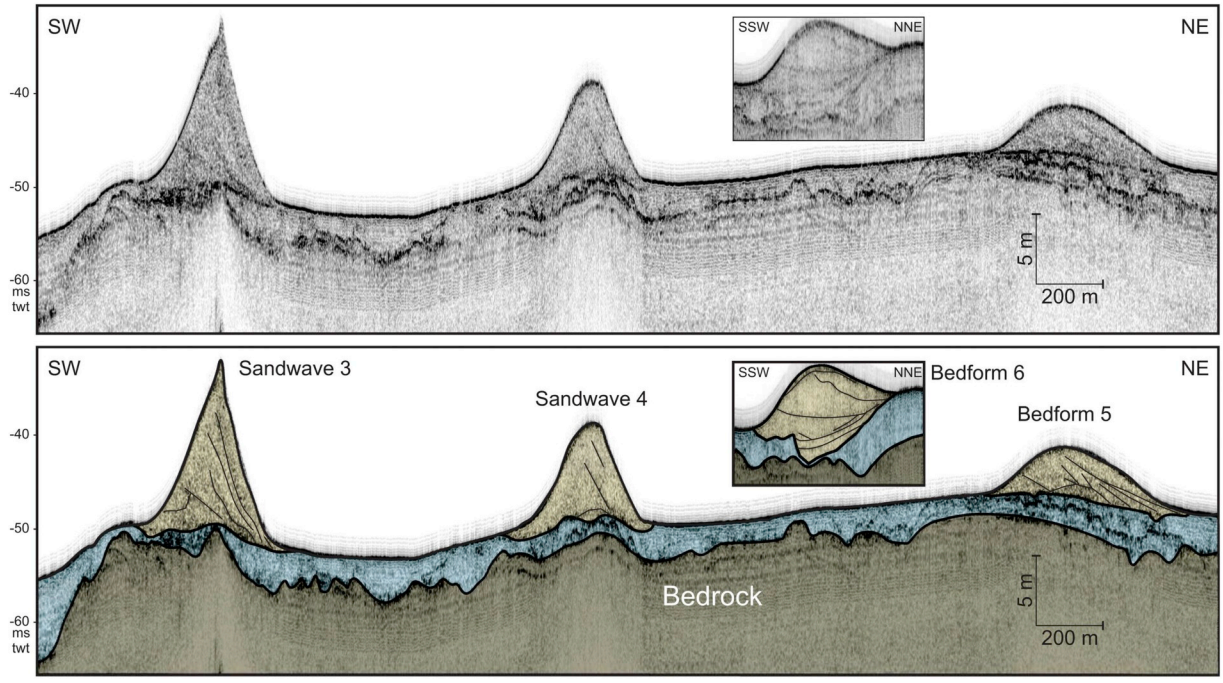

Fig. 9. Seismic profile (location in Fig. 8) across large sandwaves and bedforms (yellow) shows NE migration. Bedform 6 (small panel) shows more aggradation than progradation. Post-glacial deposits in blue and bedrock in khaki. (For interpretation of the references to colour in this figure legend, the reader is referred to the web version of this article.)

consist of gravelly sand. Sandwave surfaces are usually covered by gravelly sand (Fig. 17E), but areas with sandy gravel or sand occur on the large sandwaves. Bedrock outcrops (Fig. 17B) occur, especially in the southeast. Video observations show that ripples, megaripples and small sandwaves occur on and around sandbank A (Fig. 17C–D), even if they are not well-defined in our multibeam data. Most of the videos highlight strong current occurring in the study area, with a high concentration of particles moving in the water column.

4.6. Oceanographic data

The Svalbard-800 m model shows two clockwise gyres centered around the two shallowest areas of Spitsbergenbanken (Figs. 18A and 19). One anticlockwise gyre occurs between the two shallow areas, another further north. Tidal ellipses show current velocities up to 1 m/s on top of Spitsbergenbanken and about 70 cm/s in the study area. However, tidal-induced residual currents are low, around 2–2.5 cm/s with a general northeast direction in the study area (Fig. 18B; Gjevik et al., 1990, 1994). The tidal currents are influenced by the bank morphology but the model (12.5–25 km grid resolution) does not use detailed topography (Gjevik et al., 1990, 1994).

According to the Svalbard-800 m model, which shows bottom residual currents, maximum current speeds are 0.09–0.16 m/s in the study area (Fig. 18A). Direction of the currents varies inside the study area. The northwestern corner of the study area is dominated by currents from the west-southwest. They turn and come from the north in the sandwave area. Currents are more or less parallel to the sandbank crests while in the southeast, currents are from the north.

5. Discussion

5.1. Megaripples

Mapping of the megaripples from the 20 cm grid shows that wave megaripples dominate the northwestern part of the study area, where the sediments are coarser and the directions of the bottom currents are variable, while current megaripples are predominant in the SW-NE corridor with the sand sheets, where the current direction is more stable (Figs. 4, 15 and 20). Mean wind stress comes from the east (Weigel, 2005) and likely creates currents moving towards the east. These currents may be responsible for the formation of the NE-SW current megaripples.

Interference megaripples formed by a combination of wave energy and bottom currents mainly occur in the current megaripple corridor (Fig. 4). They form sand accumulations up to 2 m thick, which may be precursors of larger sand accumulations such as sandbanks. Interference megaripples highlight the fact that bottom currents and wave energy together are important processes for the accumulation of sand on the

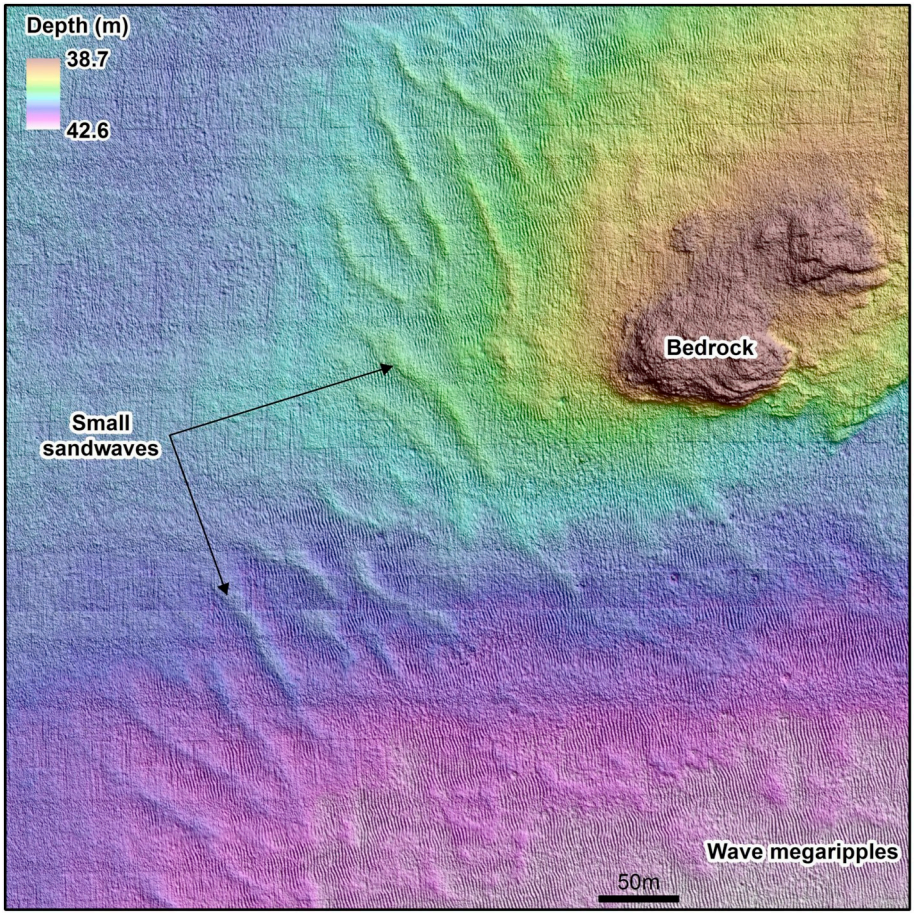

Fig. 10. Smaller sandwaves oriented NW-SE and wave megaripples (type 1). Grid size: 20 cm. See Fig. 1 for location.
Multibeam bathymetry from MAREANO (www.mareano.no).

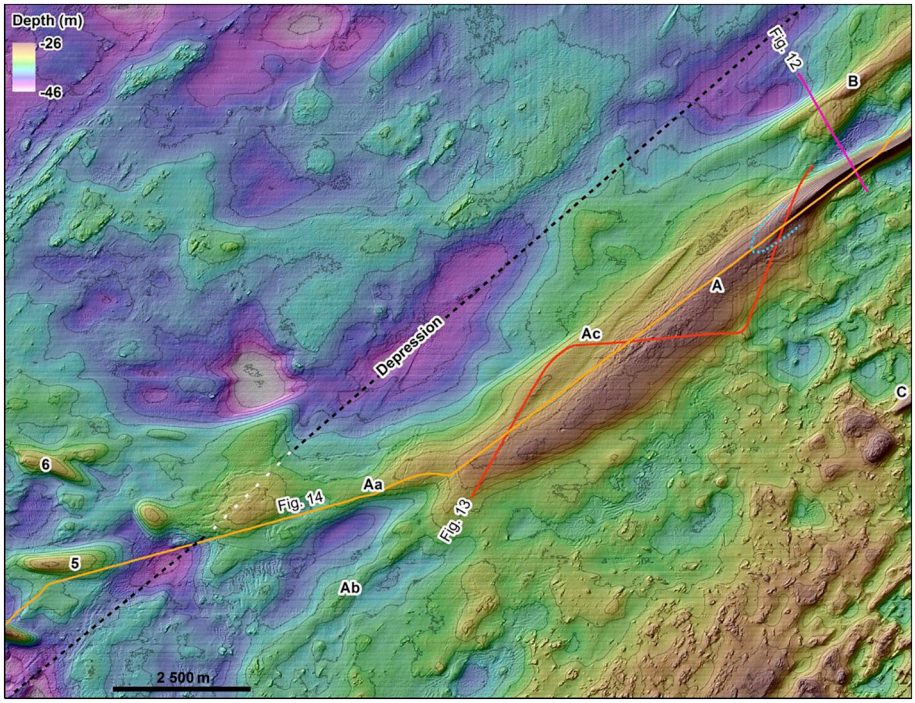

Fig. 11. Bathymetric map (5 m grid) of sandbanks A-B and bedforms 5–6. Aa and Ab represent the tail of sandbank A. Ac shows a sand accumulation north of A. The blue dotted line on A indicates approximately the boundary between the upper unit and the tail of A. Black lines are 1 m contours. See Fig. 1 for location. (For interpretation of the references to colour in this figure legend, the reader is referred to the web version of this article.)
Multibeam bathymetry from MAREANO (www.mareano.no).

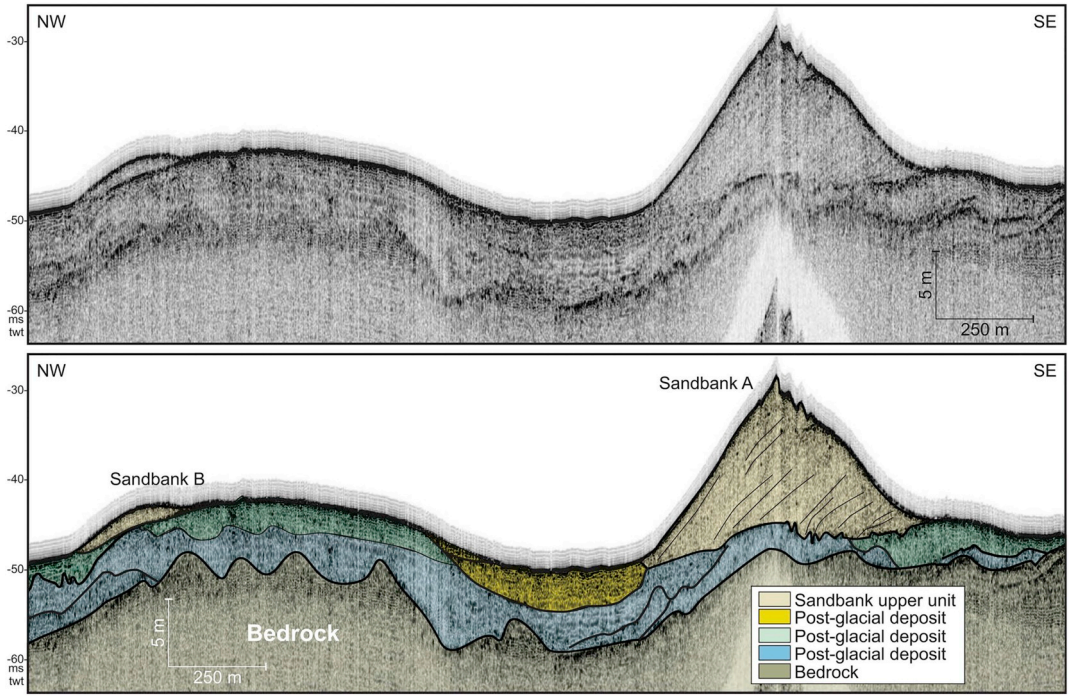

Fig. 12. Seismic profile crossing sandbanks A and B. Location in Fig. 11.

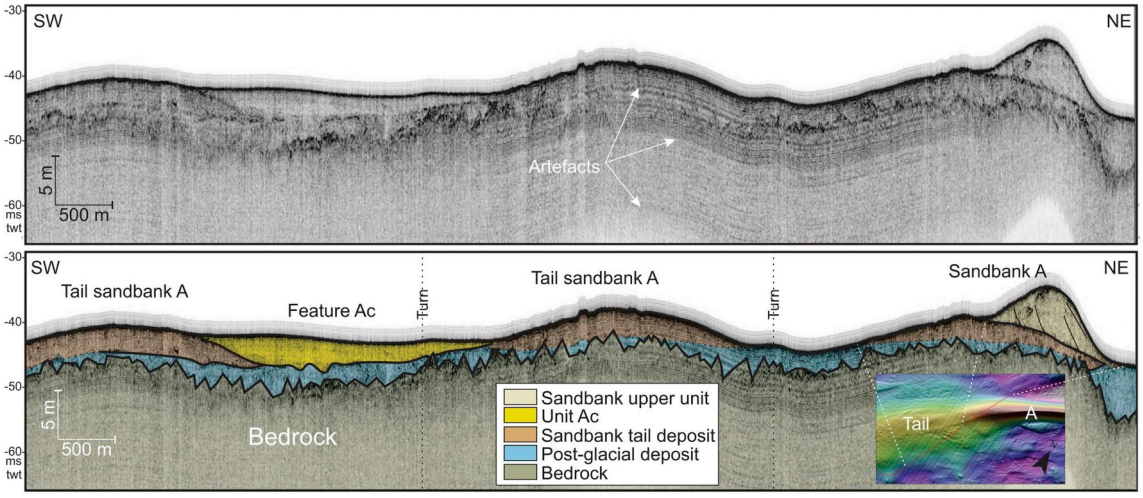

Fig. 13. Seismic line along the lowest part of sandbank A. Note that sand accumulation Ac (dark yellow) covers the tail of sandbank A (orange). Location in Fig. 11. (For interpretation of the references to colour in this figure legend, the reader is referred to the web version of this article.)

top of Spitsbergenbanken. The strength of the bottom currents varies in time, and current megaripples with NW-SE crest orientation locally cover the interference megaripples in some places (Fig. 7) indicating that the system is still not in equilibrium over some of these sand ridges.

Lingoid/lunate megaripples, mostly occurring around the large sandwaves, form under stronger current conditions than elongated straight (mostly wave) or sinuous (current) megaripples (e.g. Nichols, 1999), indicating that currents are stronger in the large sandwave area. This is in accordance with the hydrodynamical Svalbard-800 m model, as well as their migration direction (Figs. 8F and 20).

In summary, the large area covered by current megaripples and lingoid/lunate megaripples with NW-SE crest orientation show that strong currents come from the SW or the NE. Wave megaripples with N-S crest orientation indicate waves from the west or the east. Current megaripples with SE-NE crest orientation, mostly observed on the east side of sandbank A, show currents from the SE. Lack of current megaripples may indicate that currents are too strong to form megaripples, but could also indicate a lack of sand.

5.2. Sandwaves

The fields of smaller sandwaves extend north and east of the large sandwaves, indicating a decrease in current velocity and/or the availability of sand in these directions. A decrease in current energy is also confirmed by the shape of the sandwave 4 crest, which is sharp only along 250 m, while sandwaves 1 to 3 have > 1000 m long sharp crests. Moreover, some of the smaller sandwaves, especially in the north, have rounded crests indicating that they are presently inactive. Their

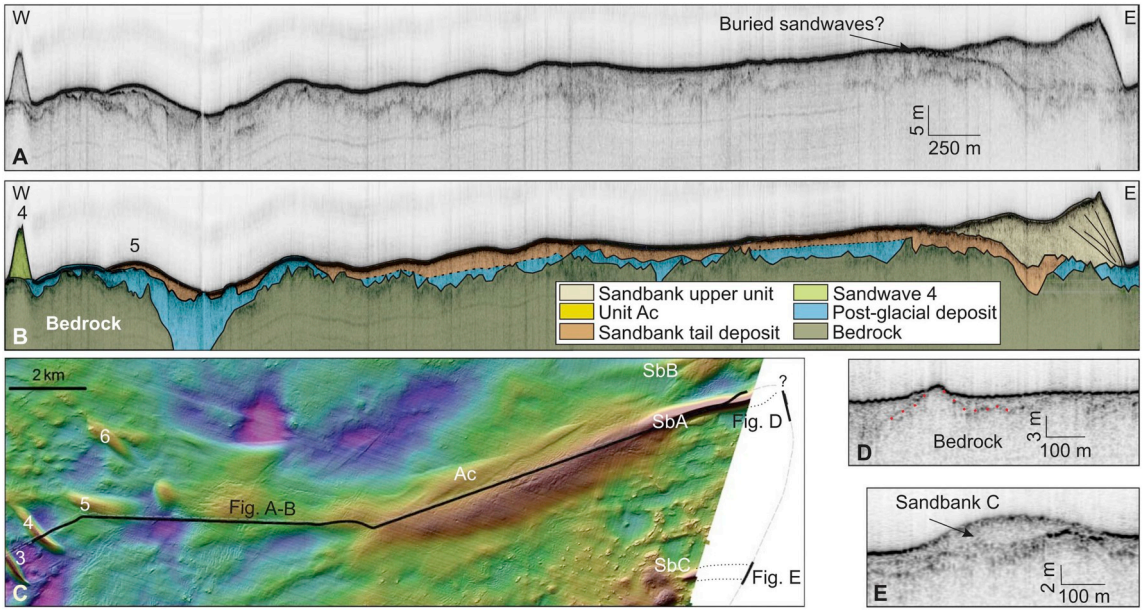

Fig. 14. Seismic line along sandbank A. The tail of sandbank A (SbA) can be traced to bedform 5. Buried sandwaves could occur below the upper unit. The sandbank A does not extend far eastwards as no sand accumulation occurs on figure D and the bedrock is very close to surface. In contrast, limited sand accumulation (Sandbank C - SbC) is observed in the south (figure E).

presence may indicate older stronger oceanographic conditions, when the currents were strong enough to transport sand far towards the north and form sandwaves. However, sharp crests of some of the smaller sandwaves indicate an active, but reduced, sediment transport in this region.

The sandwaves, megaripples and seabed sediments show sand transport and current directions both towards the southwest and the northeast. This opposition also occurs between the tidal model, showing residual currents towards the northeast around the sandwave area (Gjevik et al., 1990; Gjevik et al., 1994), and the Svalbard-800 m model showing residual currents from the north. As the large sandwaves and most of the smaller ones fit with the tidal model, they are likely of tidal origin. Smaller bedforms (lingoid/lunate megaripples surrounding the sandwaves) and the highest sandwave crests (Fig. 8D–F) indicate other currents from the northeast, which is consistent with the Svalbard-800 m model (Fig. 18A) but opposite to the tidal residual current directions. The northeast current could also be related to ebb and flood tides, as sandwave crests and ripple/megaripple migration direction can be reversed during the tidal cycle (Johnson et al., 1982). The large sandwaves would then record the strongest currents in the study area, towards the north whereas smaller bedforms record currents (tidal currents, oceanographic currents, waves) in various directions. It is interesting to note that the large sandwaves 1–4 occur where the Svalbard-800 m model shows the strongest currents (Figs. 4 and 18A).

Large sandwaves 1–4 (Fig. 8) are still active as they display sharp crests. They are located between two shallow areas (Fig. 19) with clockwise gyres. Currents passing through narrow pathways usually increase in strength, which may explain their formation at this location and their absence further north. The intensification of the bottom currents has eroded the seafloor along a SW-NE trending corridor, several metres deep, where the sandwaves occur. Sand eroded from the corridor may have accumulated both in the sandwaves and the sandbanks further east/northeast. The decrease in size and crest length of the large sandwaves northwards confirms a bottom current decrease in that direction, away from the shallow areas.

5.3. Transitional bedforms

Bedforms 5 and 6 are smaller, smoother (Fig. 8) and have internal reflections with a much lower angle than sandwaves 1–4 (Fig. 9), indicating a different origin and/or an evolution different from the large sandwaves 1–4. The bedforms are almost parallel to the flow direction of the tide (10–20° angle) and show an angle of 30° for bedform 6 and 60° for bedform 5 with the Svalbard-800 m model flow direction (Fig. 18), while crests of sandwave 1–4 are oblique to normal to the currents. Bedforms 5 and 6 were probably depositional features transitional between sandbanks, as they occur at the end of tail Aa, and large sandwaves. They are presently more longitudinal bedforms which are now moribund, eroded and smoothed by currents. They may have been attached to the older sandbank unit as sandwaves at the end of the tail unit. This pattern occurs on modern sandbanks (e.g. Franzetti et al., 2015; Schmitt and Mitchell, 2014). Then they likely have been reworked later to form two separate bedforms. The orientation of bedforms 5 and 6, when compared to sandwaves 1–4, may indicate a greater influence of waves, geostrophic currents or a turn in tidal currents. Located at the end of the sandbank tail, they also indicate a change from transverse (ripples and sandwaves) to longitudinal bedforms (sandbanks).

5.4. Sandbanks

The location of sandbank A in the middle of Spitsbergenbanken is special as it does not appear to be linked to a former coastline. However, it occurs very close to shallow areas south and east of the bank (e.g. obstacle in Fig. 19). According to Belderson et al. (1982), banner banks are solitary small sandbanks formed in proximity to a headland or a rocky shoal. Due to the proximity of sandbank A to rocky shallow areas and the relatively small size of the sandbank, it may have had a formation similar to a banner bank with eddies forming at the front of the obstacle. Banner banks are attributed to tidal eddies on either side of headlands (Kenyon and Cooper, 2005). They are usually symmetric in areas of tidal currents and asymmetric in areas of

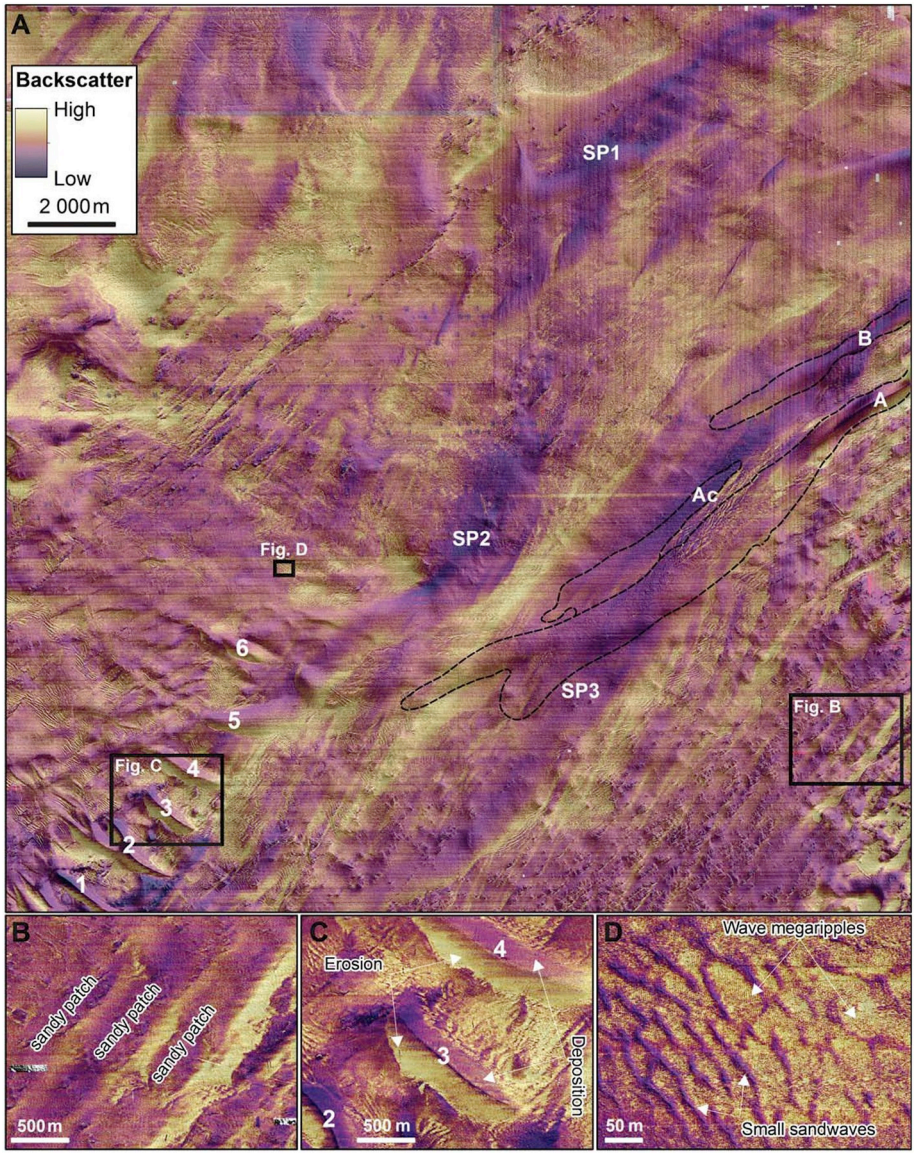

Fig. 15. Multibeam backscatter dataset. Elongated features characterized by low backscatter are marked SP1, SP2 and SP3. Most of these features are not observed in the bathymetry. See Fig. 1 for location. 1–4: large sandwaves; 5–6: other bedforms described in the text; A-C: sandbanks; Ac: sand deposit crossing the basal unit of sandbank A.
Multibeam data from MAREANO (www.mareano.no).

unidirectional flow. Sandbank B, located on the other side of the rocky area/obstacle east of sandbank A (Fig. 19), is possibly a smaller banner bank. However, the presence of an anti-clockwise eddy in the west and rocky shallower outcrops in the east of sandbank A together with strong southwest tidal currents may have also contributed to the sand accumulation in this specific location.

Sandbank A shows characteristics similar to some North Sea sandbanks, e.g. wide tail and narrow head. According to Caston (1981), the wide tail corresponds to the upstream area and the narrow head to the downstream part. This implies that the current forming sandbank A is mainly from the southwest, which is in accordance with the tidal model of Gjevik et al. (1990, 1994) and the Svalbard-800 m model (Figs. 18A and 19). At present, tidal currents reach 1 m/s on Spitsbergenbanken (Gjevik et al., 1990). An almost circular tidal ellipse (rotary current with no real dominant tidal velocities) with currents of > 70 cm/s occurs in the sandbank area. Sandbanks form where currents are c. 70–150 cm/s (Belderson et al., 1982). Tidal current speeds in the study area are in the lower range but still strong enough to form and maintain a tidal sandbank. According to Belderson et al. (1982), sandwaves start forming at c. 50–60 cm/s and large sandwaves around 70 cm/s, which also fit with the tidal current speeds in the study area. Fig. 19 shows two gyres, one clockwise and one anticlockwise, with a convergence at the sandbank location. This convergence likely maintains the sand supply towards the sandbanks.

Sand sheet SP3 (Fig. 15) crosses the tail of sandbank A, which shows a very flat and wide top (Fig. 11), indicating that this part of the sandbank is no longer active. At about 33–34 m depth (blue dotted line in Fig. 11), the tail unit is covered by the upper unit (Figs. 12–14). This upper unit has a sharp crest and occurs several metres above the tail unit. The characteristics of this upper unit indicate that the sand transport remains active today on this part of the sandbank.

Sandbank A is shaped/reshaped by modern currents. The bedforms

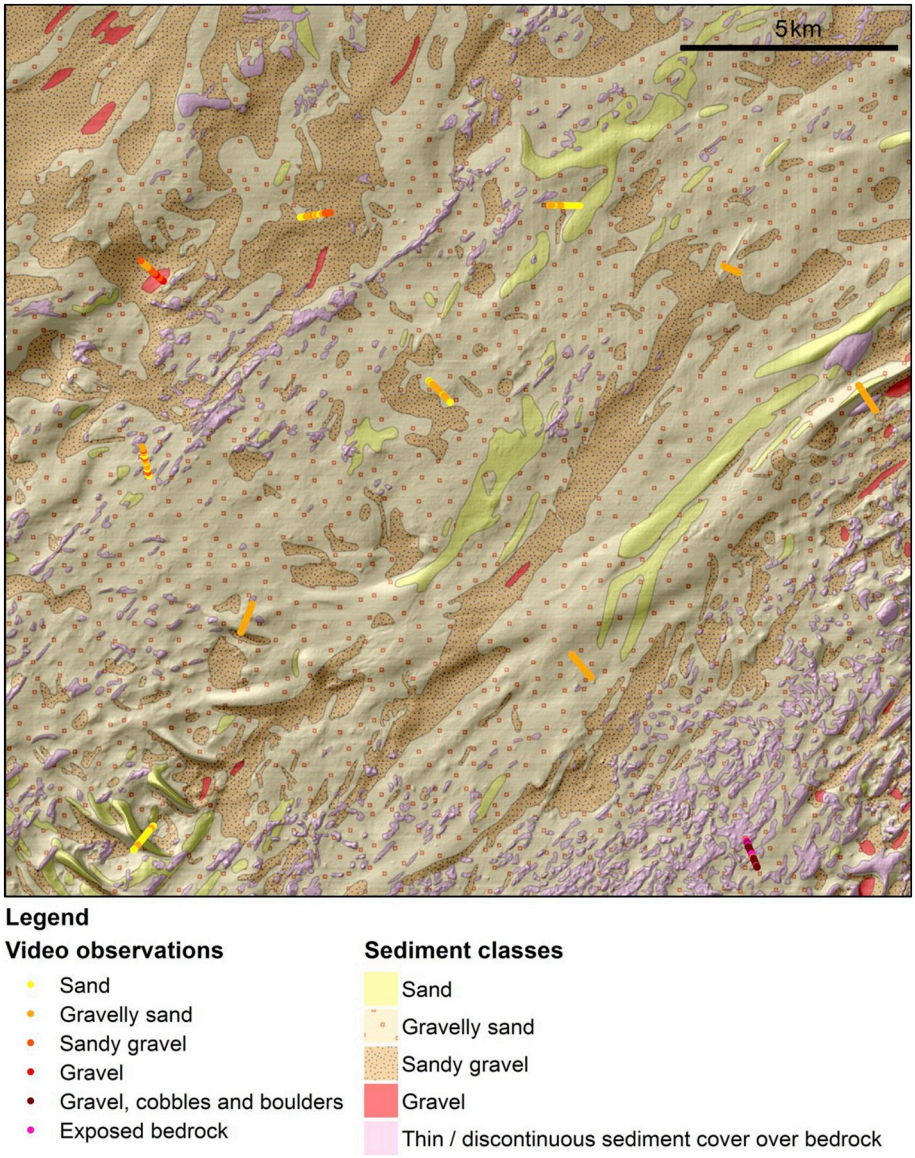

Fig. 16. Video observations and sediment grain-size map of the study area. Grid size: 5 m. See Fig. 1 for location (from Bellec et al., 2018).

and sediment types indicate a high energy environment even though the Svalbard-800 m model shows relatively low (residual) currents. The convergence of the tails (E-W Aa and SW-NE Ab) of sandbank A towards the east suggests convergence of the wave (E-W current) and southwest bottom currents in that direction, enhanced by southwest tidal currents. The orientation of SP3, covering the tail of the bank, indicates that the bottom currents have changed to a slightly more northward direction since deposition of the first unit (tail) of the sandbank.

Sandbank B is much smaller than A, possibly because sandbank A has trapped most of the sand, likely because it is closer to the sand source. Indeed, the shallow areas south of the study area may be a source of sand. This would explain why there is more sand in the southern part of the study area than in the northwest, where sandy gravel dominates. Sandbank C is located at the eastern limit of the study area and its smooth crest likely indicates a relict or moribund small sandbank.

5.5. Sand ribbons and patches

Limited sand deposits in the northwestern part of the study area may indicate a lack of sand supply. These indicate a decrease of sand transport from the south to the northeast where the transport of sand is limited. This is likely connected to the origin of sand, which appears to be supplied from south of the study area.

In the shallowest areas in the southeast, sand patches resemble sand ribbons. Sand ribbons usually form in very high energy environments with currents of 1 m/s or more (Belderson et al., 1982). As bottom currents apparently only reach c. 70 cm/s, they are probably intermediate between sand patches and sand ribbons as sand patches occur under lower current velocities. Further north, the long sand patches stretching from the southwest towards the northeast are parallel to the tidal current direction (Gjevik et al., 1990; Gjevik et al., 1994), as well as ribbon-like deposits. Ripples and megaripples at the surface of the sand patches indicate active sand transport.

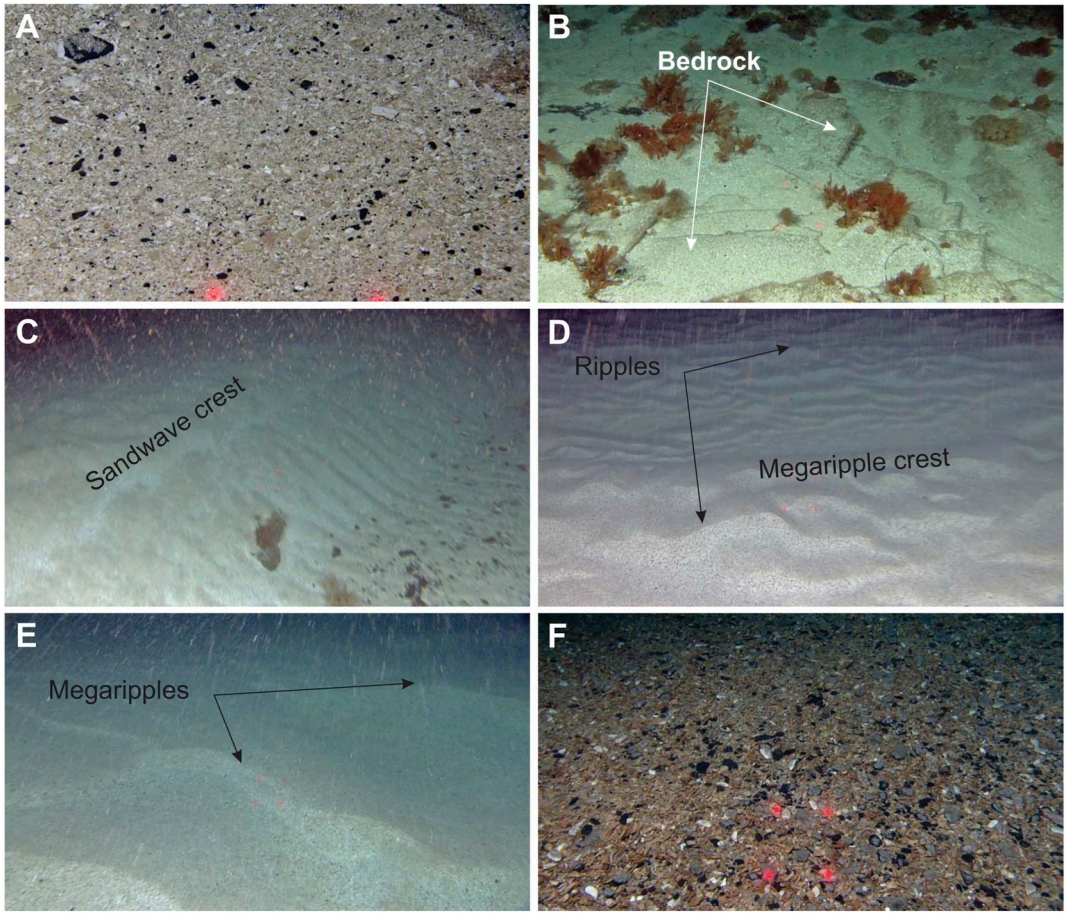

Fig. 17. Video observations. A: Shell hash/shell sand with gravel close to bedrock outcrops; B: Bedrock outcrop; C: Sandwave observed in video data but not in multibeam data; D: Ripples and NE-SW current megaripples (type 3) on top of sandbank A. Small ripples are not visible in the multibeam data; E: Megaripples (type 2) on top of sandwave 3. F: Shell hash with gravel in type 1 megaripple area. 10 cm between red laser dots. (For interpretation of the references to colour in this figure legend, the reader is referred to the web version of this article.)

5.6. Timing of the large bedforms

Rüther et al. (2012) and Lantzsch et al. (2017) interpreted an increase in bottom current strength, erosion and lag formation at Spitsbergenbanken between 11.2 and 8.8 cal. ka BP. The strong currents led to large sand accumulations on Spitsbergenbanken (Zecchin et al., 2016), in Kveithola (Bjarnadóttir et al., 2013; Rüther et al., 2012) and on the outer part of the Bear Island Trough (Jensen et al., 2002) from 8.8 cal. ka BP. A short-lasting atmospheric cooling event started at 8.8 cal. ka BP (Hald et al., 2007; Rebesco et al., 2016; Sarnthein et al., 2003). This may have strengthened the Atlantic Water inflow (Andersen et al., 2004; Ślubowska-Woldengen et al., 2008) and along with a gradual shallowing caused by glacio-isostatic rebound (Elverhøi and Henrich, 2002), caused erosion and sand transport. This sequence of events could have led to the formation of the coarse sediment layer (sandy gravel, Fig. 16) below the sandy sheets and started the erosion of the SW-NE depression from the sandwaves to the north of the sandbanks (Figs. 8A and 11).

Cores from Kveithola show that the interval 8.8–6.3 cal. ka BP is characterized by the coarsest sediments and an increase of biogenous carbonate content (Lantzsch et al., 2017). The sandbanks probably started to form during this period of extensive erosion and sand transport. These strong currents may also explain the larger extent of the sandbank during this period, as it extended to the sandwave area. The formation of the large sandwaves 1–4 as well as the transitional bedforms 5 and 6 likely also started during this period. After 7.2 cal. ka BP, an overall cooling was accompanied by a reduced inflow of Atlantic Water (Ślubowska-Woldengen et al., 2008). A decrease in grain size in the region at around 6.3 cal. ka BP might be related to this reduction in Atlantic Water inflow (Lantzsch et al., 2017). During this period, sand transport likely decreased and the first sandbank unit (tail unit) may have become moribund as well as the transitional bedforms 5 and 6 at the end of the sandbank A tail which were eroded and smoothed by bottom currents. We have no absolute ages for when the reactivation of the sandbank occurred. However, it is plausible that it was reactivated during the Neoglacial cooling about 4–2 cal. ka BP, when deteriorating climatic conditions characterized the region (Ślubowska-Woldengen et al., 2008).

5.7. Comparison with other continental shelves

5.7.1. The large sandwaves

Large sandwaves have been described on the Norwegian shelf (e.g. Hola trough, Bøe et al., 2009 with sandwaves up to 7 m high and 300 m wavelength) but also on other shelves covered by ice during the last glaciation (see Van Landeghem et al., 2009a on the Irish shelf and their comparison with the North American shelves). The large sandwaves of the Irish shelf reach up to 36 m at 91.5 m depth, the largest sandwaves

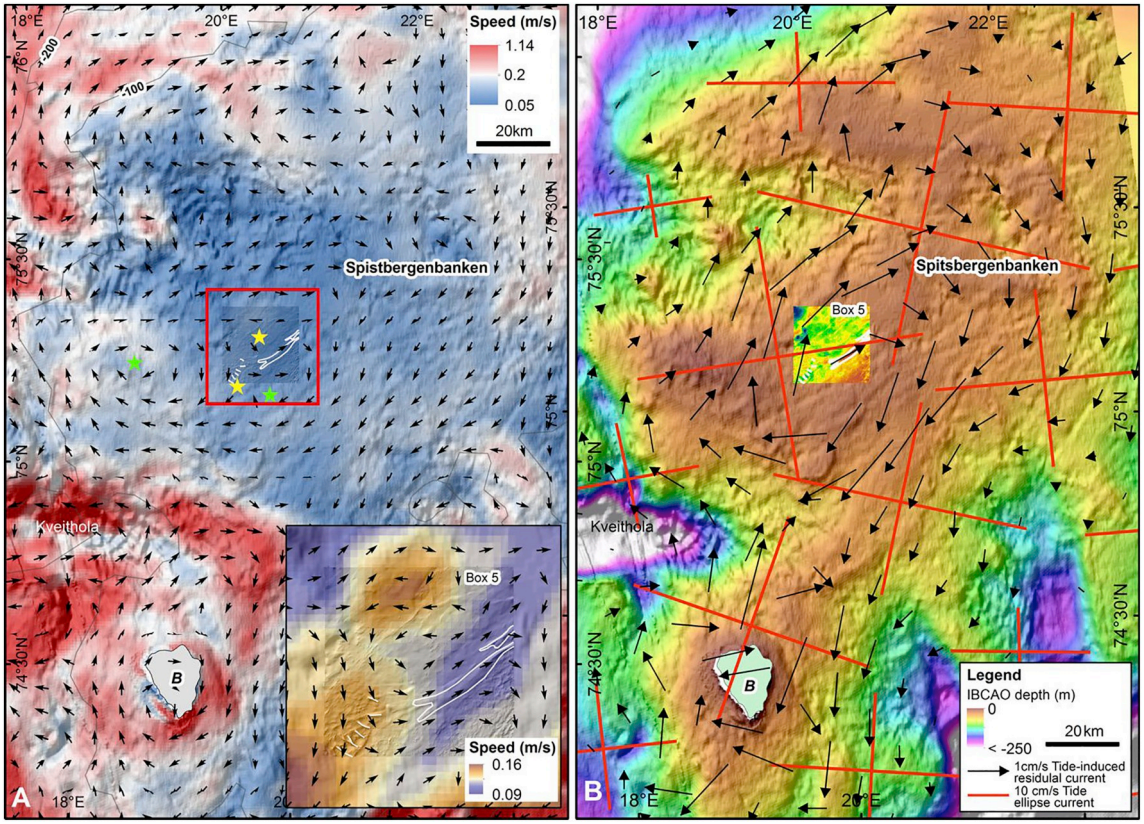

Fig. 18. Oceanography data, Spitsbergenbanken. A) Maximum speed of bottom current (m/s) from the 800 m Svalbard-800 m model. The bottom panel is a detailed view of the study area (red square in the overview panel). Black arrows show maximum current speed and direction (from the Svalbard-800 m model). Green stars mark clockwise gyres; yellow stars mark anticlockwise gyres. White lines highlight sandbanks and sandwaves. B) Tide-induced residual current from Gjevik et al. (1994), and tidal ellipses from Gjevik et al. (1990) on top of Spitsbergenbanken. B: Bjørnøya. (For interpretation of the references to colour in this figure legend, the reader is referred to the web version of this article.)
Multibeam bathymetry from MAREANO (www.mareano.no) and overview bathymetry from IBCAO (Jakobsson et al., 2012).

being symmetrical trochoidal-type (Van Landeghem et al., 2009b). These authors indicate that the large sandwaves found on the Irish and North America shelves are located in special settings: wide and shallow shelf or semi-enclosed sea or basin where tidal changes are the most noticeable during the sea level rise (North Sea: Austin, 1991; Bristol Channel and Irish Sea: Scourse and Austin, 2002), bathymetric deeps where glacio-isostatic rebound and sea-level changes are important on the North American shelves (Barrie et al., 2009). Strong bi-directional tides with (nearly) symmetrical ellipses and glacial depositional basins supplying sediments are also important factors for the formation of the large trochoidal sandwaves (Van Landeghem et al., 2009a). These authors also point out that these sandwaves were probably created under different palaeo-conditions, i.e. older stronger tidal conditions, associated with marine transgression after the last glacial maximum and then were reworked later. Smaller asymmetrical sandwaves may occur on both sides of the large sandwaves as well as on their flanks with a migration direction conforms to the new hydrological conditions.

The large sandwaves on Spitsbergenbanken show northward migration, while parts of their crests, smaller sandwaves and megaripples occasionally show opposite migration direction, possibly indicating changes in residual current directions. Strong palaeo-currents have been described for the western Barents Sea (Lantzsch et al., 2017; Rüther et al., 2012), and Spitsbergenbanken can be compared to a wide and shallow shelf with an almost symmetrical tidal ellipse (Gjevik et al., 1990, 1994). Then it is possible that the formation and the evolution of the large sandwaves on Spitsbergenbanken show similarities with the ones on the Irish shelf. If we refer to the evolution of the large sandwaves in the Irish Sea, the large sandwaves on Spitsbergenbanken could evolve into symmetrical (trochoidal) sandwaves while smaller sandwaves still highlight modern current direction.

5.7.2. *Sandbanks*

Sandbank A shows similarities with North Sea sandbanks. In their description of the Middelkerke Bank (Belgian continental shelf), Trentesaux et al. (1999) indicated that the upper unit which forms the main body of the modern bank presents two zones: one zone shows a stronger asymmetry with 1–5° dipping reflectors, and could correspond to the upper unit of sandbank A, while the second zone has a more flat shape with sub-horizontal reflectors onlapping the base of the unit and looks more like the lower unit of the sandbank A. However, Trentesaux et al. (1999) modern bank unit only shows minor bounding surfaces while the surface between sandbank A units is likely erosional. The difference could be due to the different types of seismic used (they mainly used Sparker lines in their paper), but also to a different formation process like a gap/stop/erosive period during the formation of sandbank A which did not occur during the Middelkerke bank formation. This means that the older unit of sandbank A could have had a different formation origin.

The upper unit of sandbank A resembles North Sea tidal sandbanks with a prograding facies covered by sandwaves (Balson, 1999; Houbolt, 1968; Mathys, 2009; Trentesaux et al., 1999). This indicates that the actual mechanisms of formation and/or maintenance of the modern

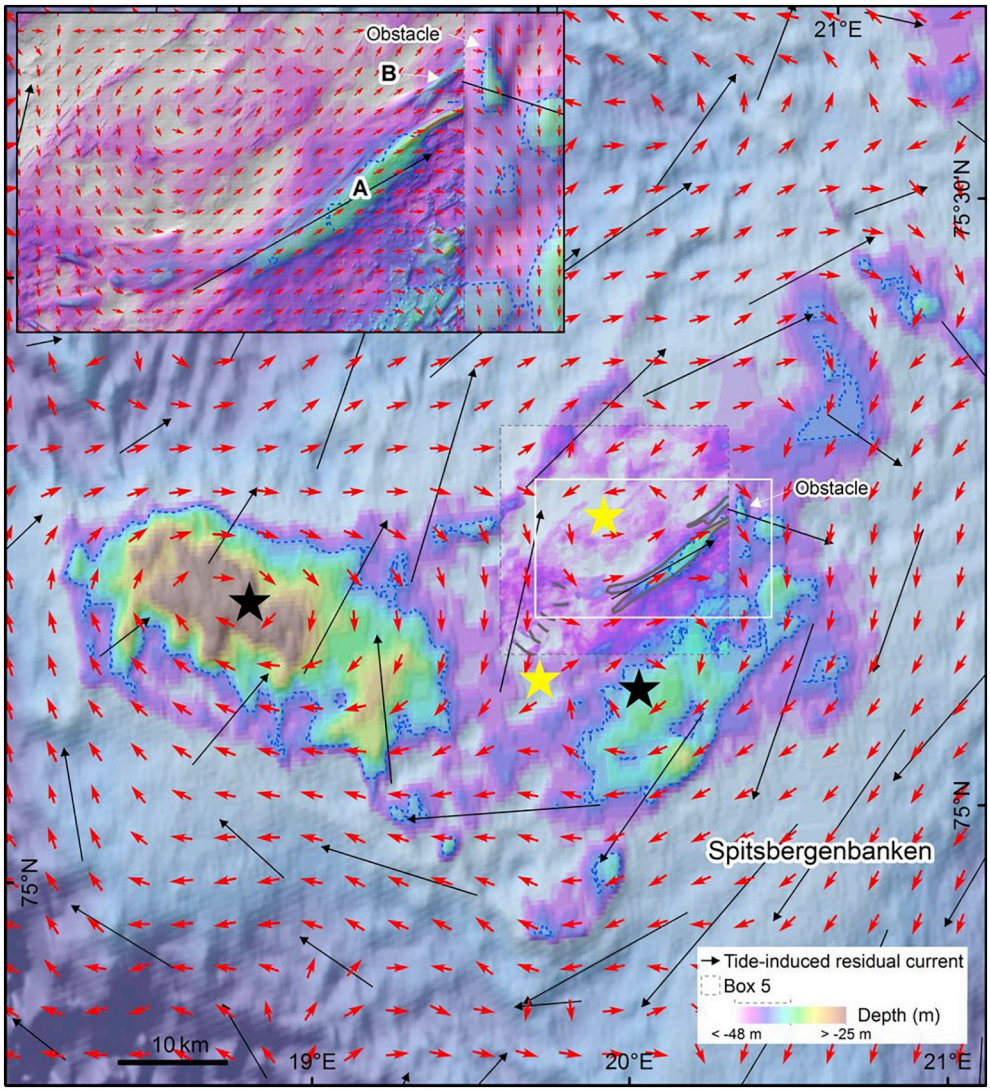

Fig. 19. Comparison of tide-induced residual currents from Gjevik et al. (1994) (black arrows) and bottom currents from the Svalbard-800 m model (red arrows). Note clockwise currents around the two shallow areas. Points where currents are turning are marked by stars (black: clockwise gyres, yellow: anticlockwise gyres). Medium and large-scale bedforms are marked with grey lines. The object "obstacle" is likely to be a rocky outcrop. Blue dotted lines: 36 m depth contour. Grid sizes: 5 (in study area) and 250 m. (For interpretation of the references to colour in this figure legend, the reader is referred to the web version of this article.)
Multibeam bathymetry from MAREANO (www.mareano.no), background bathymetry data from IBCAO (Jakobsson et al., 2012).

sandbanks are quite similar in both regions. The correlation of the lower unit with the North Sea sandbank units is more difficult to establish. In the Belgian continental shelf, storm ridges or coastal sandbanks preceded the formation of the tidal sandbanks themselves (Mathys, 2009; Trentesaux et al., 1999). This progression from storm ridges/coastal sandbanks to tide-dominated sandbanks is linked to the coastal retreat and the transgression after the last glaciation.

However, due to the isostatic rebound, the global sea level rise did not have the same effect on Spitsbergenbanken as in the North Sea. Studies from Bjørnøya show that the isostatic rebound did not exceed the sea level rise (Salvigsen and Slettemark, 1995), while studies from the southern tip of Spistbergen (Svalbard largest island) show that post-glacial emergence could have reached 19 m there (Ziaja and Salvigsen, 1995). This is supported by recent modelling from the area (Patton et al., 2017). This explains the absence of transgressive deposits below the upper unit of sandbank A similar to the ones found underneath the North Sea tidal banks (Balson, 1999; Mathys, 2009; Trentesaux et al., 1999).

6. Conclusions

This study is based on multibeam data from the shallowest part (26–53 m depth) of Spitsbergenbanken in the western Barents Sea. The exceptionally high quality and resolution of the data have allowed the identification and interpretation of megaripples (minimum height 4 cm and minimum wavelength 1 m) in unprecedented detail. Several types of megaripples are identified within the study area. Their geometry indicates that they are formed and influenced by several complex, often interacting processes including waves, tidal currents and ocean currents. The interaction of processes is reflected in bedform size, crest style, grain size, spatial distribution and migration pattern.

In addition to wave and current megaripples, we observed interference megaripples, which to our knowledge have not previously been described from a bank setting. These megaripples form by the convergence of different currents, here wave and bottom currents, and indicate an on-going sand accumulation process. Although the sand supply and/or the bottom currents appears to be insufficient and incapable, respectively, to create such large sandbanks as the ones described in the east of the study area, the presence of interference megaripples may indicate the onset of future sandbanks.

Four large sandwaves occur in a SW-NE trending depression between two shallow areas, which likely focus and increase the strength of the bottom currents. The initial erosion of the depression probably occurred around 8–9 cal. ka BP, but the sandwaves are presently maintained by tidal residual currents from the southwest. The presence of the shallow areas south of the sandwaves seems to be a prerequisite for the sandwave formation as large sandwaves do not occur elsewhere in the study area. The sandwaves are still active and highlight the action of complex current patterns which have changed since the onset of the sandwave formation. They may evolve in the future in more

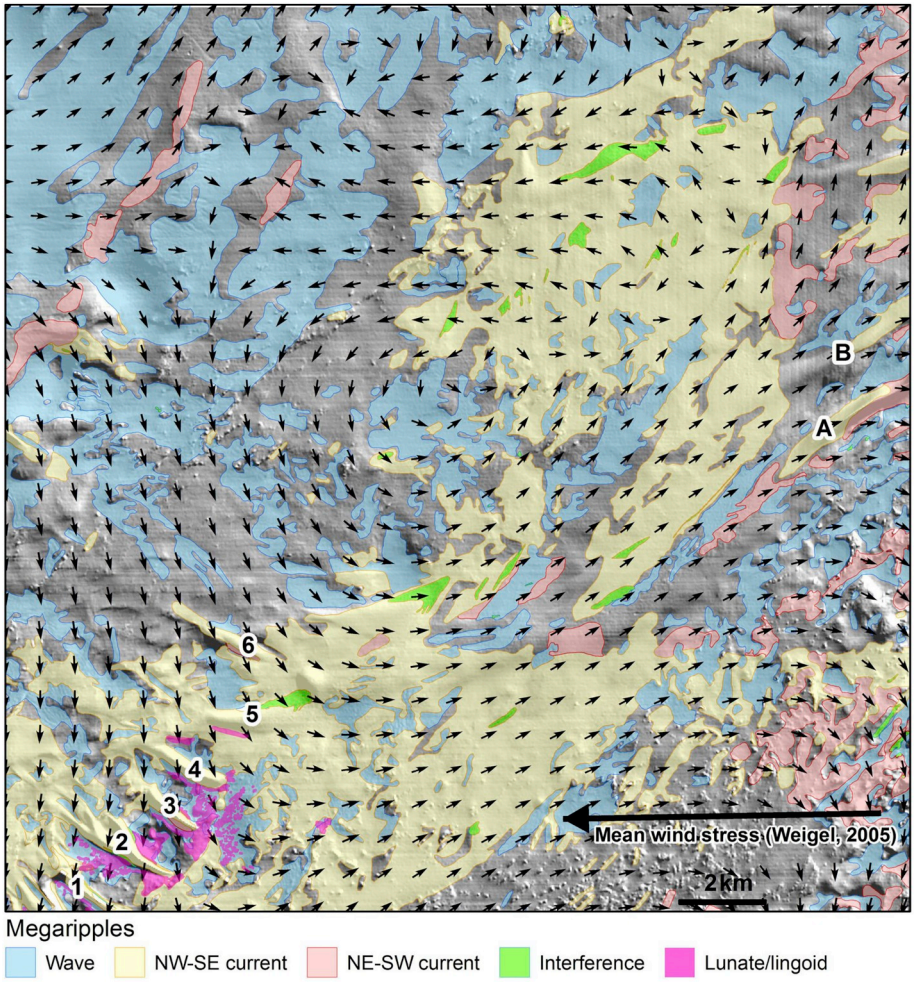

Fig. 20. Comparison between the location of the different types of megaripples and the bottom current from the Svalbard-800 m model. Mean wind stress (Weigel, 2005) coming from east.

symmetrical trochoidal shape.

Three sandbanks are formed by the convergence of tidal and bottom currents. The orientation of the sandbanks is in accordance with modelled bottom currents. The largest sandbank may have started to form around 8–9 cal. ka BP when bottom currents were stronger than today. The basal unit of the largest sandbank likely became moribund as a result of lower current strength at about 6.3 cal. ka BP. The sandbank was reactivated later, and it is plausible that this coincided with the Neoglacial cooling during the late Holocene (4–2 cal. ka BP).

The ripples, megaripples, sandwaves and sandbanks indicate a very high energy environment with enough sand to form and maintain these bedforms. Spitsbergenbanken is a unique environment characterized by bedforms linked to multiple seabed processes operating at different spatial and temporal scales.

Acknowledgements

We acknowledge all participants of the MAREANO programme (www.mareano.no) for invaluable cooperation. The multibeam data were acquired and supplied by NHS. The data is released under a Creative Commons Attribution 4.0 International (CC BY 4.0): https://creativecommons.org/licenses/by/4.0/. The 2018 TOPAS data were acquired through a NGV project funded by Lundin Norge AS.

References

Andersen, C., Koç, N., Jennings, A., Andrews, J.T., 2004. Nonuniform response of the major surface currents in the Nordic Seas to insolation forcing: implications for the Holocene climate variability. Paleoceanography 19 (2), PA2003.

Ashley, G., 1990. Classification of large-scale subaqueous bedforms: a new look at an old problem. J. Sediment. Petrol. 60 (1), 160–172.

Austin, R.M., 1991. Modelling Holocene tides on the NW European continental shelf. Terra Nova 3, 276–288.

Balson, P., 1999. The Holocene coastal evolution of eastern England: evidence from the offshore Southern North Sea. In: Kraus, N.C., McDougal, W.G. (Eds.), Coastal Sediments, Proceedings of 4th International Symposium of the American Society of Civil Engineers, pp. 1284–1294.

Barrie, J.V., Conway, K.W., Picard, K., Greene, H.G., 2009. Large scale sedimentary bedforms and sediment dynamics on a glaciated tectonic continental shelf: examples from the Pacific margin of Canada. Cont. Shelf Res. 29, 796–806.

Belderson, R.H., Johnson, M.A., Kenyon, N.H., 1982. Bedforms. In: Stride, A.H. (Ed.), Offshore Tidal Sands: Processes and Deposits. Chapman and Hall, London.

Bellec, V.K., Van Lancker, V., Degrendele, K., Roche, M., Le Bot, S., 2010. Geo-environmental characterization of the Kwinte Bank. J. Coast. Res. 51, 63–76.

Bellec, V., Elvenes, S., Lepland, A., Chand, S., Dolan, M., Bjarnadóttir, L. R., Bøe, R., Rise, L., Thorsnes, T. & Selboskar, O.H., 2018. Geologisk havbunnskart, Kart 75001900, April 2018. M 1: 100 000. Norges geologiske undersøkelse.

Bjarnadóttir, L.R., Rüther, D.C., Winsborrow, M.C.M., Andreassen, K., 2013. Grounding-line dynamics during the last deglaciation of Kveithola, W Barents Sea, as revealed by seabed geomorphology and shallow seismic stratigraphy. Boreas 42, 84–107.

Bøe, R., Bellec, V.K., Dolan, M.F.J., Buhl-Mortensen, P., Buhl-Mortensen, L., Slagstad, D., Rise, L., 2009. Giant sandwaves in the Hola glacial trough off Vesterålen, North Norway. Mar. Geol. 267, 36–54.

Bøe, R., Skarðhamar, J., Rise, L., Dolan, M.F.J., Bellec, V.K., Winsborrw, M., Skagseth, Ø., Knies, J., King, E.L., Walderhaug, O., Chand, S., Buenz, S., Mienert, J., 2015. Sandwaves and sand transport on the Barents Sea continental slope offshore northern Norway. Mar. Pet. Geol. 60, 34–53.

Buhl-Mortensen, P.B., Buhl-Mortensen, L., Dolan, M., Dannheim, J., Kröger, K., 2009. Megafaunal diversity associated with marine landscapes of northern Norway: a preliminary assessment. Nor. J. Geol. 89, 163–171.

Caston, G.F., 1981. Potential gain and loss of sand banks in the Southern Bight of the North Sea. Mar. Geol. 41, 239–250.

Collins, M.B., Shimwell, S.J., Gao, S., Powell, H., Hewitson, C., Taylor, J.A., 1995. Water and sediment movement in the vicinity of linear sandbanks: the Norfolk Banks,

southern North Sea. Mar. Geol. 123, 125–142.
Egbert, G.D., Erofeeva, S.Y., 2002. Efficient inverse modeling of barotropic ocean tides. J. Atmos. Ocean. Technol. 19 (2), 183–204.
Elvenes, S., Bøe, R., Rise, L., 2016. Post-glacial sand drifts burying De Geer moraines on the continental shelf off North Norway. In: Dowdeswell, J.A. (Ed.), Atlas of Submarine Glacial Landforms: Modern, Quaternary and Ancient. Geological Society, London, Memoirs, vol. 46. pp. 261–262.
Elverhøi, A., Henrich, R., 2002. 13 - past glaciomarine environments. In: Menzies, John (Ed.), Modern and Past Glacial Environments. Butterworth-Heinemann, Oxford, pp. 391–415.
Franzetti, M., Le Roy, P., Garlan, T., Graindorge, D., Sukhovich, A., Delacourt, C., Le Dantec, N., 2015. Long term evolution and internal architecture of a high-energy banner ridge from seismic survey of Banc du Four (Western Brittany, France). Mar. Geol. 369, 196–211.
Gjevik, B., 2008. Tides and topographic waves in the vicinity of the Svalbard islands in the Barents Sea. In: DNVA-RSE Norway-Scotland Internal Waves Symposium, Oslo 14–15 October 2008, (extended abstract).
Gjevik, B., Nøst, E., Straume, T., 1990. Atlas of Tides on the Shelves of the Norwegian and Barents Seas. University of Oslo, Oslo (74 p).
Gjevik, B., Nøst, E., Straume, T., 1994. Model simulations of the tides in the Barents Sea. J. Geophys. Res. 99 (C2), 3337–3350.
Hald, M., Andersson, C., Ebbesen, H., Jansen, E., Klitgaard-Kristensen, D., Risebrobakken, B., Salomonsen, G.R., Sarnthein, M., Sejrup, H.P., Telford, R.J., 2007. Variations in temperature and extent of Atlantic Water in the northern North Atlantic during the Holocene. Quat. Sci. Rev. 26 (25–28), 3423–3440.
Hattermann, T., Isachsen, P.E., von Appen, W.-J., Albretsen, J., Sundfjord, A., 2016. Eddy-driven recirculation of Atlantic water in Fram Strait. Geophys. Res. Lett. 43 (7), 3406–3414.
Houbolt, J.J.H.C., 1968. Recent sediments in the Southern Bight of the North Sea. Geol. Mijnb. 47, 245–273.
Hughes, A.L.C., Gyllencreutz, R., Lohne, Ø.S., Mangerud, J., Svendsen, J.I., 2016. The last Eurasian ice sheets – a chronological database and time-slice reconstruction, DATED-1. Boreas 45, 1–45.
Jakobsson, M., L. A. Mayer, B. Coakley, J. A. Dowdeswell, S. Forbes, B. Fridman, H. Hodnesdal, R. Noormets, R. Pedersen, M. Rebesco, H.-W. Schenke, Y. Zarayskaya A, D. Accettella, A. Armstrong, R. M. Anderson, P. Bienhoff, A. Camerlenghi, I. Church, M. Edwards, J. V. Gardner, J. K. Hall, B. Hell, O. B. Hestvik, Y. Kristoffersen, C. Marcussen, R. Mohammad, D. Mosher, S. V. Nghiem, M. T. Pedrosa, P. G. Travaglini, and P. Weatherall, 2012. The International Bathymetric Chart of the Arctic Ocean (IBCAO) version 3.0, Geophys. Res. Lett. 39.
Jensen, H.K.B., Hald, M., Vorren, T., 2002. Norwegian Petroleum Directorate gravity cores from the Barents Sea - core quality assessment and list of cores transferred to NGU. NGU Report 2002.064, 31 p.
Johnson, M.A., Kenyon, N.H., Belderson, R.H., Stride, A.H., 1982. Sand transport. In: Stride, A.H. (Ed.), Offshore Tidal Sands: Processes and Deposits. Chapman and Hall, London.
Kenyon, N.H., Cooper, B., 2005. Sand banks, sand transport and offshore wind farms. CGK MarineGeo Report, 106 p.
King, E.L., Bøe, R., Bellec, V.K., Rise, L., Skarðhamar, J., Ferré, B., Dolan, M.F.J., 2014. Contour current driven continental slope-situated sandwaves with effects from secondary current processes on the Barents Sea margin offshore Norway. Mar. Geol. 353, 108–127.
Lantzsch, H., Hanebuth, T.J.J., Horry, J., Grave, M., Rebesco, M., Schwenk, T., 2017. Deglacial to Holocene history of ice-sheet retreat and bottom current strength on the western Barents Sea shelf. Quat. Sci. Rev. 173, 40–57.
Lepland, A., Rybalko, A., Lepland, A., 2014. Seabed Sediments of the Barents Sea. Scale 1:3 000 000.
Loeng, H., 1989. Ecological features of the Barents Sea. In: Rey, L., Alexander, V. (Eds.), Proceedings of the Sixth Conference of the Comité Arctique International, 13–15 May 1985. E. J. Brill, Leiden, pp. 327–365.
Mathys, M., 2009. The Quaternary Geological Evolution of the Belgian Continental Shelf, Southern North Sea. PhD thesis. Ghent University, Belgium (454 p).
Nichols, G., 1999. Sedimentology and Stratigraphy. Blackwell, Oxford.
Ottesen, D., Dowdeswell, J., 2009. An inter-ice glaciated margin: submarine landforms and a geomorphic model based on marine-geophysical data from Svalbard. GSA Bull. 121, 1647–1665.
Patton, H., Hubbard, A., Andreassen, K., Auriac, A., Whitehouse, P.L., Stroeven, A.P., Shackleton, C., Winsborrow, M., Heyman, J., Hall, A.M., 2017. Deglaciation of the Eurasian ice sheet complex. Quat. Sci. Rev. 169, 148–172.
Rasmussen, T.L., Thomsen, E., Skirbekk, K., Ślubowska-Woldengen, M., Klitgaard Kristensen, D., Koç, N., 2014. Spatial and temporal distribution of Holocene temperature maxima in the northern Nordic seas: interplay of Atlantic-, Arctic- and polar water masses. Quat. Sci. Rev. 92, 280–291.
Rebesco, M., Özmaral, A., Urgeles, R., Accettella, D., Lucchi, R.G., Rüther, D., Winsborrow, M., Llopart, J., Caburlotto, A., Lantzsch, H., Hanebuth, T.J.J., 2016. Evolution of a high-latitude sediment drift inside a glacially-carved trough based on high-resolution seismic stratigraphy (Kveithola, NW Barents Sea). Quat. Sci. Rev. 147, 178–193.
Reineck, H.-R., Singh, I.B., 1980. Depositional Sedimentary Environments, second edition. Springer, New York.
Risebrobakken, B., Dokken, T., Smedsrud, L.H., Andersson, C., Jansen, E., Moros, M., Ivanova, E.V., 2011. Early Holocene temperature variability in the Nordic Seas: the role of oceanic heat advection versus changes in orbital forcing. Paleoceanography 26, PA4206.
Rüther, D.C., Bjarnadóttir, L.R., Junttila, J., Husum, K., Rasmussen, T.L., Lucchi, R.G., Andreassen, K., 2012. Pattern and timing of the northwestern Barents Sea Ice Sheet deglaciation and indications of episodic Holocene deposition. Boreas 41, 494–512.
Salvigsen, O., Slettemark, Ø., 1995. Past glaciation and sea levels on Bjørnøya, Svalbard. Polar Res. 14 (2), 245–251.
Sarnthein, M., Van Kreveld, S., Erlenkeuser, H., Grootes, P.M., Kucera, M., Pflaumann, U., Schulz, M., 2003. Centennial-to-millennial-scale periodicities of Holocene climate and sediment injections off the western Barents shelf, 75° N. Boreas 32 (3), 447–461.
Schmitt, T., Mitchell, N.C., 2014. Dune-associated sand fluxes at the nearshore termination of a banner sand bank (Helwick Sands, Bristol Channel). Cont. Shelf Res. 76, 64–74.
Scourse, J.D., Austin, W.E.N., 2002. Quaternary shelf sea palaeoceanography: recent developments in Europe. Mar. Geol. 191, 87–94.
Skogseth, R., Haugan, P.M., Jakobsson, M., 2005. Watermass transformations in Storfjorden. Cont. Shelf Res. 25, 667–695.
Slagstad, D., McClimans, T.A., 2005. Modelling the ecosystem dynamics of the Barents Sea including the marginal ice zone: I. Physical and chemical oceanography. J. Mar. Syst. 58, 1–18.
Ślubowska-Woldengen, M., Koç, N., Rasmussen, T.L., Klitgaard-Kristensen, D., Hald, M., Jennings, A.E., 2008. Time-slice reconstructions of ocean circulation changes on the continental shelf in the Nordic and Barents Seas during the last 16,000 cal. yr BP. Quat. Sci. Rev. 27 (15), 1476–1492.
Trentesaux, A., Stolk, A., Berné, S., 1999. Sedimentology and stratigraphy of a tidal sand bank in the southern North Sea. Mar. Geol. 159, 253–272.
Van Landeghem, K.J.J., Uehara, K., Wheeler, A.J., Mitchell, N.C., Scourse, J.D., 2009a. Post-glacial sediment dynamics in the Irish Sea and sediment wave morphology: data-model comparisons. Cont. Shelf Res. 29, 1723–1736.
Van Landeghem, K.J.J., Wheeler, A.J., Mitchell, N.C., 2009b. Variations in sediment wave dimensions across the tidally dominated Irish Sea, NW Europe. Mar. Geol. 263, 108–119.
Weigel, K., 2005. On the Wind Stress and Air-Ice Interactions Over the Barents Sea. Doctoral dissertation. Christian-Albrechts-Universität (84 p).
Zecchin, M., Rebesco, M., Lucchi, R.G., Caffau, M., Lantzsch, H., Hanebuth, T.J.J., 2016. Buried iceberg-keel scouring on the southern Spitsbergenbanken, NW Barents Sea. Mar. Geol. 382, 68–79.
Ziaja, W., Salvigsen, O., 1995. Holocene shoreline displacement insouthernmost Spitsbergen. Polar Res. 14, 339–340.